이학석사학위논문

Three-Dimensional Geologic Modeling of the Pohang Basin Distributed in Haedo-Dong, Nam-Gu, Pohang-Si, Korea

한국 포항시 남구 해도동 일대에 분포하는 포항분지의 삼차원 지질 모델링

2013년 2월

서울대학교 대학원

지구환경과학부

안 해 성

Three-Dimensional Geologic Modeling of the Pohang Basin Distributed in Haedo-Dong, Nam-Gu, Pohang-Si, Korea

한국 포항시 남구 해도동 일대에 분포하는 포항분지의 삼차원 지질 모델링

지도교수 김 준 모

이 논문을 이학석사학위논문으로 제출함

2013년 2월

서울대학교 대학원

지구환경과학부

안 해 성

안해성의 석사학위논문을 인준함

2013년 2월

위 원 장 _____ (인)

부 위 원 장 _____ (인)

위 원 _____ (인)

Abstract

Three-Dimensional Geologic Modeling of the Pohang Basin Distributed in Haedo-Dong, Nam-Gu, Pohang-Si, Korea

Hae-Sung Ahn

School of Earth and Environmental Sciences

The Graduate School

Seoul National University

Three-dimensional geologic modeling for quantitative characterization and realistic visualization in the Pohang Basin, Korea is performed by using GOCAD (geological object computer aided design) software. The study area is located in entire Haedo-Dong, Nam-Gu, Pohang-Si, Gyeongsangbuk-Do, Korea and is long in the east-west direction 1,200 m, the south-north direction 2,200 m, and 2,176 m depth. Geographic information systems (GIS) and borehole (A, B, C, DS-1, DS-2, PY-2, 301, and 302) data are collected and analyzed first. As a result, the study area is composed of the cretaceous igneous rocks, tertiary continental sediments,

and marine sediments. The cretaceous igneous rocks are classified into the plutonic rocks and volcanic rocks, and the tertiary marine sediments are classified into the Hakrim, Heunghae, Idong, and Duho Formation. Meanwhile, there is no fault structure in this study area. First, through the primary analysis of raw data, three-dimensional structural modeling is performed by using discrete smooth interpolation (DSI) algorithm. Then, three-dimensional grid model composed of total 2,046,000 deformable cells is then constructed and three-dimensional geologic formation modeling is performed by integrating three-dimensional structural model and three-dimensional grid model. In addition, in order to estimate and analyze the distribution of lithofacies in uninvestigated area, variogram modeling and three-dimensional lithofacies modeling is performedin 100 times by using sequential indicator simulation (SIS) and truncated Gaussian simulation (TGS). In this case, since the cretaceous plutonic rocks, volcanic rocks, and tertiary continental sediments compose of granite, tuff and conglomerate as single lithofacies, respectively, three-dimensional lithofacies modeling is performed only of the tertiary marine sediments including Hakrim, Heunghae, Duho, and Idong Formation. Three-dimensional lithofacies modeling simulation results show that the mudstone is distributed remarkably much more in comparison to the sandstone in the tertiary marine sediments. In addition, according to result of statistics analysis, the result of TGS shows that sandstone is distributed

in relatively smaller ratio compared with the result from SIS. In addition, the ratio of mudstone and sandstone used in SIS is similar to raw data than TGS. To assess the quality of the results of three-dimensional lithofacies modeling, Cross-validation is performed. As a results of cross-validation, it is confirmed that the deep borehole PY-2 among the six boreholes indicate the highest level of dependence for three-dimensional lithofacies modeling.

Keywords: Pohang Basin, three-dimensional geologic modeling, geostatistic, sequential indicator simulation, truncated Gaussian simulation, cross-validation

***Student Number*: 2011-20371**

Contents

List of Tables

List of figures

1. Introduction

Recently, a research on deep geologic formation, such as resources exploration, carbon dioxide storage, radioactive waste disposal, geothermal energy development, and others have attracted much attention. For research on deep geologic formation, it is important to make precise assumption of geologic formation, lithofacies, and rock mass properties. Accordingly, drilling investigation is used naturally since it is the most precise method to gather such information. However, a sufficient drilling investigation is often not carried out due to constraints such as investigation expense, labor, time and other factors. In addition, there is limitation in obtaining underground information (Koo et al., 2006). To overcome this type of problems, research on three-dimensional geologic modeling for three-dimensional visualization and quantitative characterization of underground space is being conducted widely through geostatistical methods.

Three-dimensional geologic modeling is established by utilizing GIS information, such as satellite photograph, geologic map, numerical map, and others, and geophysical exploration and borehole data that includes geologic boundary and rock mass properties. This type of modeling is largely comprised of four phases. First, the process that expresses and analyzes geologic boundary and fault structure condition in three-dimensional method by using basic data structure such as point, line, triangulated surface, and others model is called three-dimensional structural modeling. It is possible for complex stratigraphic analysis,

geologic structure analysis, and others.

Second, the process that completes spatial distribution with volume by using grid structure based on three-dimensional structural model is called three-dimensional grid modeling. Third, the process that visualizes in three-dimensional way by reflecting geographical features or geologic feature properties to the model integrated three-dimensional grid model and three-dimensional structural model is called three-dimensional geologic formation modeling.

Lastly, the process that estimates and analyzes rock mass properties, such as lithofacies, porosity, permeability, and others is called three-dimensional lithofacies modeling and three-dimensional property modeling. All these processes include three-dimensional geologic modeling and research on deep geologic formation should be preceded by various researches based such technologies.

Recently, various researches of three-dimensional geologic modeling have been conducted by using geostatistical method. First of all, in order to analyze structural characteristics of sedimentary basin, three-dimensional structural modeling was performed (e.g., Guyonnet-Benaize et al., 2010; Vilain 2010). These researches primarily analyzed borehole, satellite photograph, ground surface geologic map, numerical information, and etc. In addition, performed three-dimensional structural modeling of geologic and fault by using discrete smooth interpolation (DSI) algorithm (Mallet, 1989). And three-dimensional grid and geologic formation modeling reflecting geographical features and geologic and geologic

features was also performed (e.g., Gwak and Lee, 2001; Kaufmann et al., 2009; Zanchi et al., 2009). These research suggested methodology to perform modeling. In addition, three-dimensional property modeling was performed in order to predict spatial distribution of ore body or geologic formation (e.g., Kim and Park, 2009; Kim et al., 2010; Wang and Huang, 2012). This research was conducted by using inverse distance weighting (IDW) (Shepard, 1968) of interpolation method, and kriging (Matheron, 1963) algorithm. Meanwhile, interpolation method predicts one result that is deterministic of same condition. This method has the shortcoming of not able to handle uncertainty of production. Therefore, conditional simulation of stochastic method was suggested in order to supplement shortcoming of interpolation. Typical conditional simulation used in geostatistics consists of sequential Gaussian simulation (SGS), sequential indicator simulation (SIS), and truncated Gaussian simulation (TGS) (Journel, 1974; Matheron et al., 1987; Deutsch and Journel, 1992). Meanwhile, this method was performed in order to evaluate prediction and uncertainty of distribution of geologic formation, lithofacies and rock mass properties quantitatively (e.g., Koo and Jeon, 2005; Almeida, 2010; Jeong and Jang, 2011). So far, in Korea, there is no research performed of three-dimensional geologic modeling by using three-dimensional structure, grid, geologic formation, lithofacies, and physical property modeling comprehensively.

The purpose of this study is to conduct three-dimensional geologic modeling for quantitative characterization and realistic visualization about geologic formation and lithofacies distribution in the Pohang Basin, Korea.

Therefore, in this study, GIS and borehole data is utilized and analyzed first, then three-dimensional structure, grid, geologic formation, and lithofacies modeling is performed next. Finally, cross-validation is performed.

2. Methodology

2.1. Discrete smooth interpolation

Discrete smooth interpolation was suggested by Mallet (Mallet, 1989). The method is to compute the location of unsampled nodes and able to interpolate both the physical properties and the location (x, y, z) of each node defining the geological objects in three-dimensional space. The algorithm has been especially designed for modeling natural and complex subsurface geological structures, taking into account a wide range of data as well as their complexity and variability (Meng, et al., 2009). Thus, the resulting geometry appears smooth and close to the data (Galera et al., 2003).

The basic idea of this method is to interpolate a function z, at each node β of a discrete model. The interpolation is conducted by computing a solution that honors, in the least square, a set of linear relationships between function values, also called constraints. DIS constraints can be classified into three parts. First, the roughness constraint ensures the smoothness of the results. Second, the control node constraint specifies the

value of the function at a given node of the discrete model. Last, the fuzzy equality constraints specify some linear relationship between the function values at several nodes of the discrete model. These constraints are resolved the least square sense and can be balanced with weighting coefficients. The discrete smooth interpolation is expressed as follows (Fetel and Caumon, 2008):

$$\sum_{\beta \in \Omega} A_c(\beta) z(\beta) \approx b_c \tag{2.1}$$

where β is a node of the underlying discrete model, Ω is the set formed by all the nodes while $A_c(\beta)$ and b_c are coefficients specific to the constraint c.

2.2. Blocking method

Three-dimensional geologic model typically contain finite element mesh such as hexahedron cell. These model, which are referred to as fine grid models, geostatistical models or simply geocellular models, represent geologic variation on very fine scale of raw data but their areal resolution is still relatively coarse. Therefore, fine grid geologic model can be expected to grow further, so the need for reliable upscaling techniques is required (Louis, 2005).

Blocking method is used for gridding and upscaling and can calculate

statistics from blocked data of raw data such as property, permeability or lithofacies data. There are three methods for upscaling: (1) nearest to cell center method (Fig. 1a). (2) largest proportion method (Fig. 1b) and (3) random method (Fig. 1c). The nearest to cell center method uses raw data values closest to the center of the cell being estimated. The largest proportion method uses raw data values of the most frequent occurrence in each cell and the random method uses one of the raw data values at random. Fig.1 shows schematic diagram of the blocking methods.

2.3. Variogram

A variogram is a function that describes the degree of spatial dependence of an intrinsic random function. It is calculated as the variance of the increment from two random variables at locations. Usually, the first step in any experimental variogram estimation is calculating the relative variogram values from the sampled dataset (Goovaerts P et al., 1997). Conventionally, when the variogram values are calculated, the next step is to define parameters such as the number of lags and the lag distance that will serve to establish a set of lag vectors. The vriogram is estimated by Matheron (Matheron, 1963):

$$2\gamma(h) = E\left[\left(z(x) - z(x+h)\right)^2\right] \tag{2.2}$$

where $2\gamma(h)$ is variogram function. The function of practical interest is

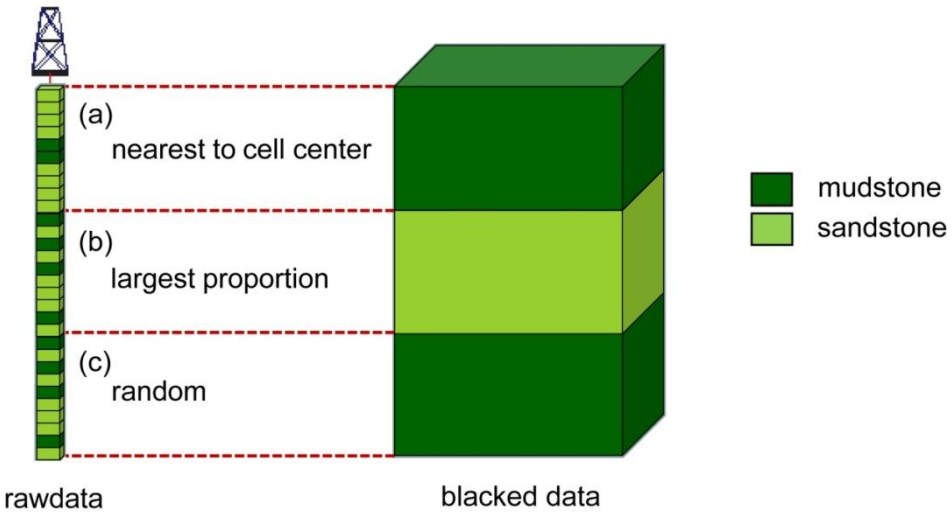

Figure 1. Schematic diagram of the blocking methods: (a) nearest to cell center, (b) largest proportion, and (c) random.

named the semi-variogram, $\gamma(h)$, and is one-half of the variogram function. Usually, this function alone is used to implement kriging. In this study, the expression $\gamma(h)$ will be referred to as the semi-variogram at a given lag distance, h, $z(x)$ and $z(x+h)$ the observed values of z at x and $x+h$.

When the available data is sampled over a regular pattern, the lag vectors in the variogram values are easy to identify. For determination of the theoretical variogram model, variogram modeling follows the classical steps: (1) searching for anisotropies in different directions, and (2) fitting of an experimental model to points, usually with a spherical, Gaussian or exponential model (Christakos, 1984). The three models and the functions are examined as follows:

(1) Spherical model is expressed as follows:

$$\gamma(h) = C_0\left[1.5\frac{h}{a} - 0.5\frac{h^3}{a^3}\right], \qquad for\ (0 \le h < a) \tag{2.3}$$

$$\gamma(h) = C_0, \qquad for\ (a \le h) \tag{2.4}$$

where C_0 is the sill and a is the range. The spherical model actually reaches the specified sill value at finite range. The tangent to this semi-variogram at the origin intersects the sill at two-thirds of the range. The

model is not permissible for a space with a dimension larger than 3.

(2) Gaussian model is expressed as follows:

$$\gamma(h) = C_0\left[1 - \exp\left(-3\left(\frac{h}{a}\right)^2\right)\right], \qquad for\ (h \le a) \tag{2.5}$$

the sill is approached asymptotically. A practical rule is to consider the range to be the distance$a$, for which the semi-variogram is $0.95C_0$. A graph of the model shows a parabolic form near the origin.

(3) Exponential model is expressed as follows:

$$\gamma(h) = C_0\left[1 - \exp\left(-\frac{3h}{a}\right)\right], \qquad for\ (h \le a) \tag{2.6}$$

the model also approaches the sill asymptotically. A practical definition of the range is the distance a where the semi-variogram is $0.95\,C_0$. Geometrically, a tangent at the origin intersects the asymptote C_0 at lag a/3. Fig. 2 shows these three models.

2.4. Conditional simulation

2.4.1. Sequential indicator simulation

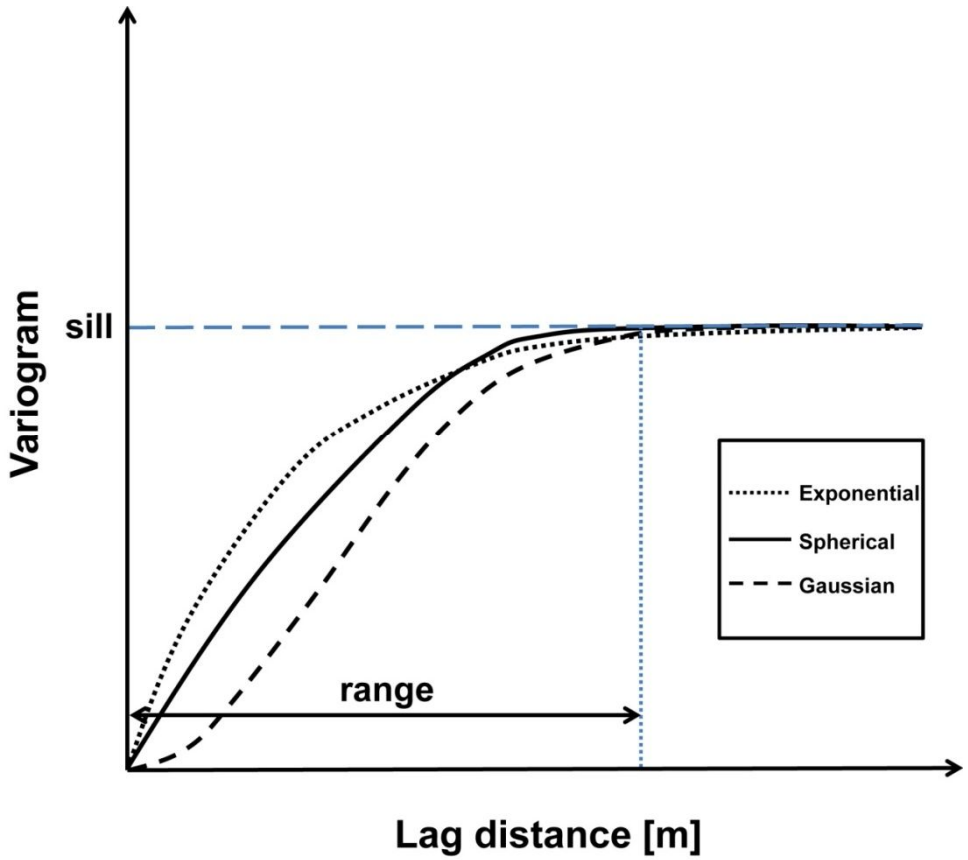

Figure 2. Curve of a variogram models showing the sill and the range.

Sequential indicator simulation algorithms, which is one of the conditional simulation methods is based on a sequential simulation approach. This includes all data available within a neighborhood including the original data and all previously simulated values. The objective is to generate a joint realization at the uninvestigated locations. SIS is performed by using the indicator kriging (IK) estimator for modeling discrete property like lithofacies. The IK estimator is examined as follows:

The observed values $\mathrm{z}(x)$ are transformed into indicator codes by the indicator function $I(x; z_k)$, which is under a desired cutoff value z_k:

$$I(x; z_k) = \begin{cases} 0, & \text{if } \mathrm{z}(x) > z_k \\ 1, & \text{if } \mathrm{z}(x) \leq z_k \end{cases} \tag{2.7}$$

Then, the semi-variogram of $\gamma_I(h)$ is used to express the spatial structure of indicator codes, written as follows:

$$\gamma_I(h) = \frac{1}{2N(h)} \sum_{i=1}^{N(h)} [I(x_i; z_k) - I(x_i + h; z_k)]^2 \tag{2.8}$$

where h is the distance between both locations,$x_i$and $x_i + h$, and $N(h)$ is the number of pairs for x_i and $x_i + h$. The conditional cumulative distribution function (ccdf), $F[z_k; x'|(n)]$, at the uninvestigated location x' can be obtained by the IK estimator:

$$F[z_k; x'|(n)] = I^*(x'; z_k) = \sum_{i=1}^{n} \lambda_i I(x_i; z_k) \quad (2.9)$$

where λ_i are the weights and (n) is the set of n observed data points used.

2.4.2. Truncated Gaussian simulation

The truncated Gaussian simulation algorithms, which is one of the conditional simulation methods relies on the truncation of a single Gaussian random field (GRF) in order to generate realizations of lithofacies. The main feature is the reproduction of the indicator variograms associated with the lithofacies and the hierarchical contact relationship among them. This method is adequate for deposits where the lithofacies exhibit a hierarchical spatial distribution, such as depositional environments or sedimentary formations (Matheron et al., 1987). The truncated Gaussian simulation is expressed as follows:

$$z(x) = \sum ik_x(x)\,, \qquad a_{i-1} < Y(x) \leq a_i \quad (2.10)$$

where $z(x)$ is the indicator function for the facies at point x, k_i is the indicator function for the 1^{th} random set, $Y(x)$ is Gaussian value at point x, and a is the threshold of the Gaussian values.

3. Study area

3.1. Location, topography and geology

Study area is located in Nam-Gu, Pohang-Si, Gyeongsangbuk-Do, Korea and adjacent to the East Sea with north latitude 36° 00′ ~ 36° 10′ and east longitude 129° 15′ ~ 129° 25′ (Fig.3). Geologic features of study area occupy most of the Pohang Basin, comprises of geologic formation of tertiary period Miocene Yonil group including Chunbuk, Hakrim, Heunghae, Idong, Duho, and Yonam Formation (Fig.3). These formations include some continental sediments deposits, but are mainly semi-consolidated and detrital sedimentary rock type of marine environment origin consisting of sandstone, mudstone, and conglomerate. Since hardness is low, it mostly is composed of semi-consolidated or unconsolidated formation (Lee et al., 2008). In entire Chilpo region, the northern side of the Pohang Basin, basic volcanic rocks appear. In addition, while formations are being accumulated, there is interpenetration of basalt from some areas and alluvium consists of sedimentary formation including mainly gravel and sand. Meanwhile, entire layer thickness of Yonil group is known as over 1000 m (Hwang, 1993; Sohn et al., 2001). Besides, there is no fault structure in this study area. According to drilling investigation conducted from 1960 to 1970, vertical distribution of Yonil group spreads to maximum 875 m from ground surface. Meanwhile, it is confirmed that Heunghae of western the Pohang Basin is noticeably shallow with 110 m. Formations of Yonil group show making of strike of south-north direction

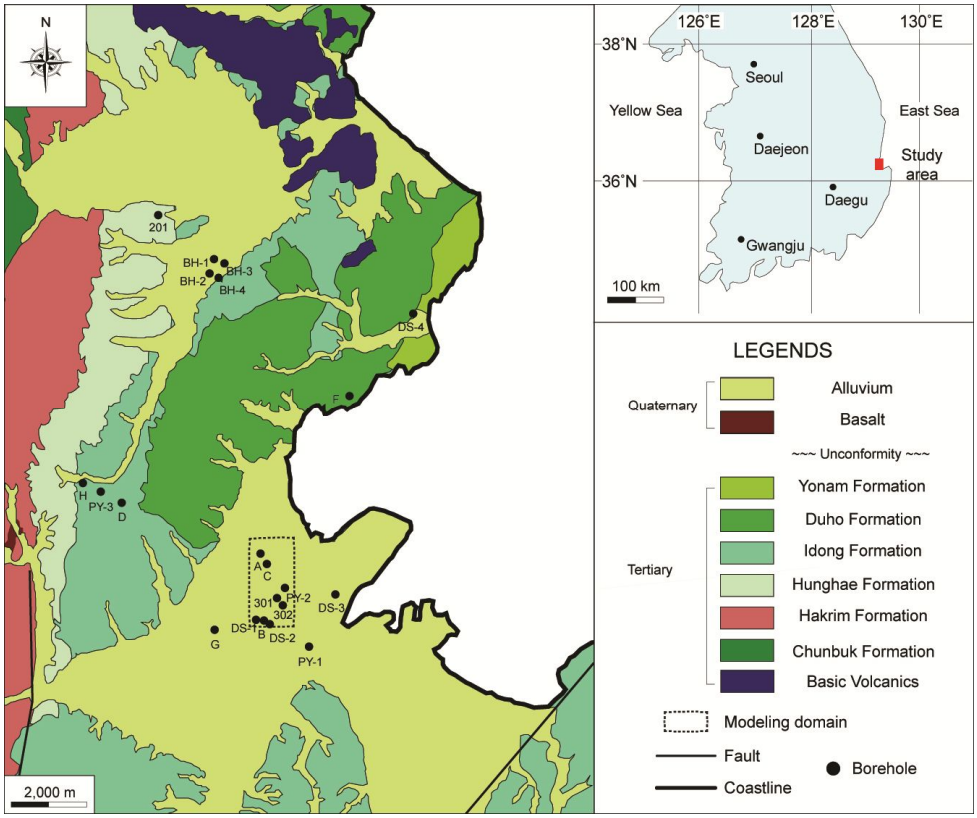

Figure 3. Location and geologic maps of the Pohang Basin with locations of 22 deep boreholes (modified from Lee et al., 2008).

and 5° ~ 10° slope to the east side (Lee et al., 2009).

3.2. Modeling domain

For a study of three-dimensional geologic modeling on deep formation, a drilling investigation that is the most precise method is used naturally because it is important to make precise assumption about geologic distributions, lithofacies, and rock mass properties. Therefore, deep borehole data are collected in the Pohang Basin to set modeling area first. Collected deep borehole data are from eighteen deep boreholes (201, 301, 302, PY-1, PY-2, PY-3, A, B, C, D, E, F, G, H, DS-1, DS-2, DS-3, DS-4) (Korea Office of Geologic Survey, 1967; Korea Institute of Energy Research, 1987) investigated for purpose of evaluation of petroleum abundance possibility in the Pohang Basin from 1960 to 1970, and from four deep boreholes (BH-1, BH-2, BH-3, BH-4) investigated with purpose of great depth geothermal existing in entire Heunghae of the Pohang city (Korea Institute of Geoscience and Mineral Resources, 2003, 2004, 2005, 2006) (Fig.4). In this study, the concentrated eight boreholes (A, B, C, DS-1, DS-2, PY-2, 301, 302) among the twenty-two deep boreholes are used in order to establish three-dimensional geologic modeling with high credibility. Thus, the modeling domain including the concentrated eight boreholes is located in entire Haedo-Dong, Nam-Gu, Pohang-Si, Gyeongsangbuk-Do, Korea and is long in the east-west direction 1,200 m, the south-north direction 2,200 m, and 2,176 m depth with eight boreholes (Fig.3).

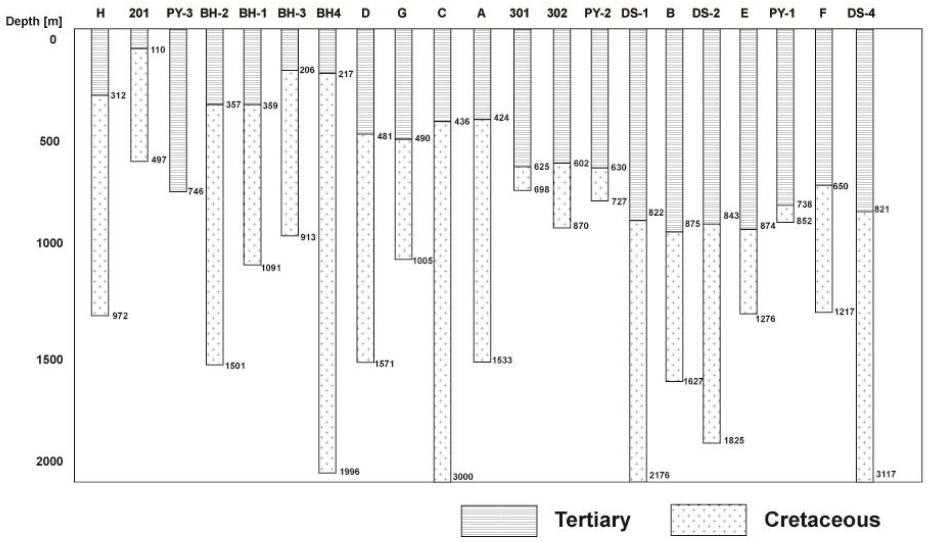

Figure 4. Stratigraphic cross-section of the 22 boreholes in the Pohang Basin (modified from Han et al., 1986).

4. Three-dimensional geologic modeling

As mentioned above, three-dimensional geologic modeling is performed for quantitative characterization and realistic visualization of geologic formations and lithofacies distribution in the Pohang Basin, Korea. For these modeling, software called GOCAD (geological object computer aided design) is used in this study. GOCAD software is based on DSI algorithm and able to create georeferenced curves, surfaces and volumes. In addition, it is a geologic feature modeling software that provides geologic structure analysis, grid model production, seismic exploration data analysis, geostatistics analysis and etc. Therefore, this is useful to three-dimensional geologic modeling in various fields related to geologic features such as mine development, geothermal energy development, radioactive waste disposal, carbon dioxide storage, and etc.

In this study, based on detailed geologic field data surveyed in the Pohang Basin such as numerical map, marine chart, geologic map and borehole data are studied by this software.

4.1. Workflow

In order to make it clear of the concept of three-dimensional geologic modeling in this study, methodology is defined as shown in following Fig.5. The first step of the proposed methodology concerns the creation of a geological database which includes the numerical map including the topographic map and marine chart (Fig.5a), geologic map (Fig. 5b), and cross-section of the boreholes (Fig.5c).The topographic data is composed

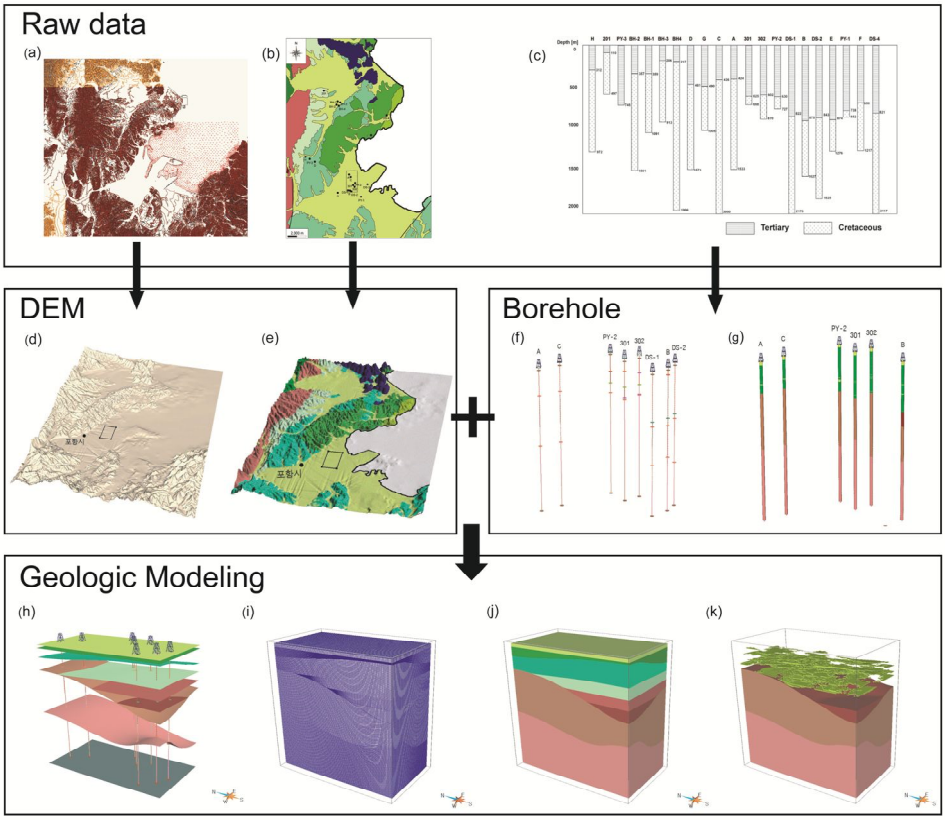

Figure 5. Workflow chart for three-dimensional geologic modeling through data integration with (a) numerical map, (b) geological map, (c) cross-section of the boreholes, (d) DEM, (e) three-dimensional geologic map, (f) boreholes data with boundary surface, and (g) boreholes data with lithofacies. Three-dimensional geologic modeling include (h) three-dimensional structural modeling, (i) three-dimensional grid modeling, (j) three-dimensional geologic formation modeling, and (k) three-dimensional lithofacies modeling.

of two-dimensional elevation contour lines and the marine chart is composed of single points with elevation values. The geologic map and the cross-section of the boreholes data represent stratigraphic boundaries and lithofacies information. Next, by using these data, basic raw data for three-dimensional geologic modeling is generated. The raw data include a digital elevation model (DEM) (Fig.5d and 5e) and the newly reinterpreted boreholes data for stratigraphic boundary and lithofacies information (Fig.5f and 5g). Then, with these raw data, three-dimensional geologic modeling including three-dimensional structural modeling (Fig.5h), three-dimensional grid modeling (Fig.5i), and three-dimensional geologic formation modeling (Fig.5j), and three-dimensional lithofacies modeling (Fig.5k) is performed.

4.2. Analysis of raw data

Raw data including the eight deep boreholes (A, B, C, DS-1, DS-2, PY-2, 301, 302), geologic map, topographic map, and marine chart are analyzed in order to generate an input data for three-dimensional geologic modeling. First, according to the boreholes data analysis, it is confirmed that geologic formation within modeling area appears to be the cretaceous igneous rock, tertiary continental and marine sediments. Moreover, the cretaceous igneous rock is classified as plutonic rocks and volcanic rocks, tertiary marine sediments are also classified as the Hakrim, Heunghae, Idong, and Duho Formation. Furthermore, in lithofacies within modeling area, the cretaceous geologic formation is composed of granite and tuff

and the tertiary geologic formation is composed of conglomerate, mudstone, and sandstone, respectively. These borehole data are computerized to generate an input data for three-dimensional geologic modeling. Fig. 6 shows the computerized deep boreholes. Especially, Fig. 6b shows only six deep boreholes because deep borehole DS-1, DS-2 does not include lithofacies information in study area. The analyzed borehole data regarding stratigraphic boundaries and lithofacies information is summarized in Table 1. Next, the DEM (Fig. 7) is constructed by numerical map including topographic map and marine chart. The DEM is constructed by interpolating the topographic data composed of two-dimensional elevation contour lines and the marine chart composed of single points with elevation values. After having obtained the DEM, three-dimensional geologic map is obtained (Fig. 8).

4.3. Results of three-dimensional geologic modeling

4.3.1. Three-dimensional structural modeling

In this three-dimensional structural modeling, the DEM of the alluvium upper surface is generated through the previously performed analysis of raw data and geologic formation boundary information obtained by eight deep boreholes (A, B, C, DS-1, DS-2, PY-2, 301, 302). Then, triangulated three-dimensional geologic formation upper surfaces are constructed by using the interpolation method to construct three-dimensional structural model. With the exception of an alluvium upper

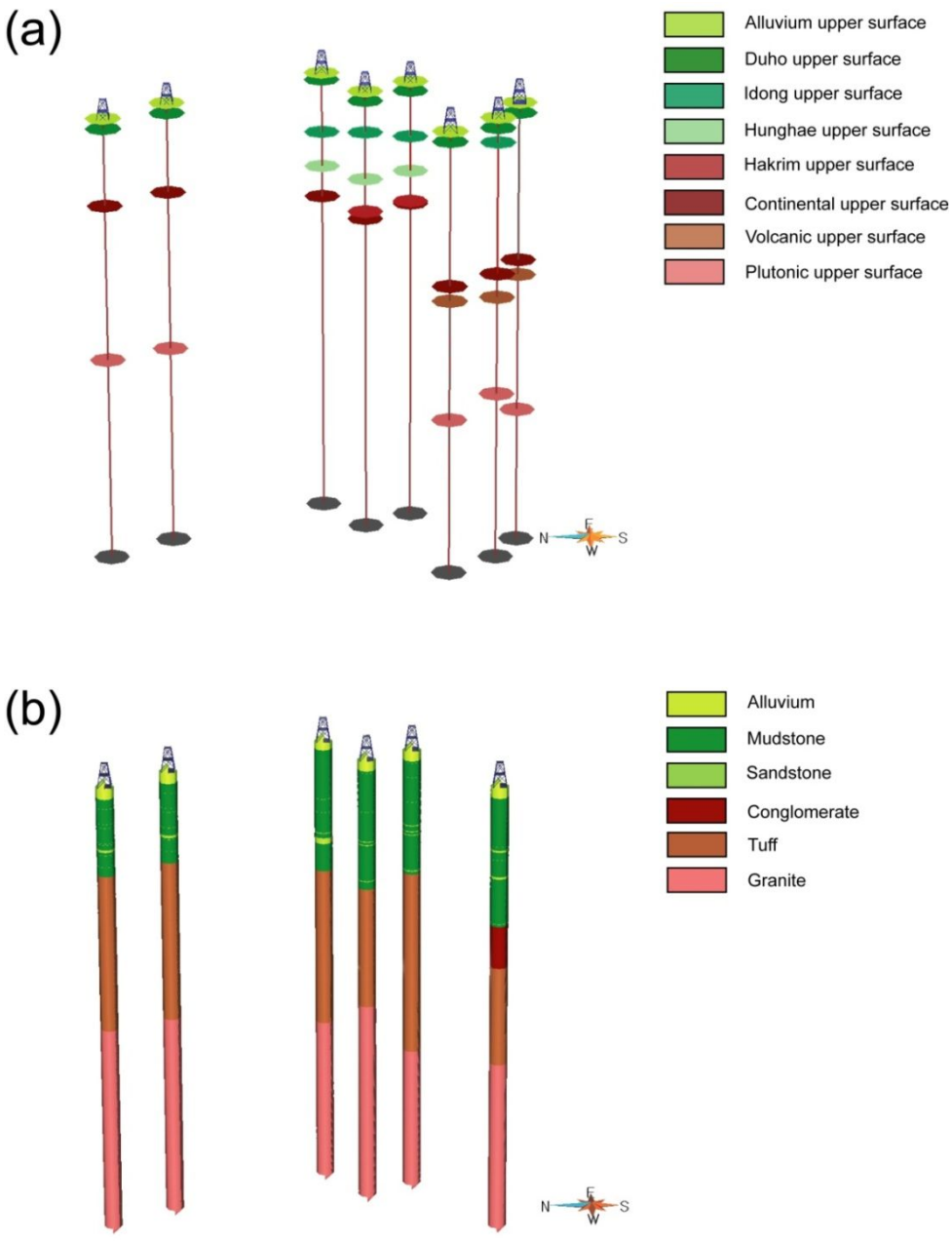

Figure 6. The computerized deep boreholes for (a) geologic formation upper surfaces and (b) lithofacies.

Table 1. Stratigraphic sequence of study area.

Period	Stratigraphic unit	Rock type
Quaternary	Alluvium	
Tertiary	~~~ Unconformity ~~~	
	Duho Formation	Sandstone, Mudstone
	Idong Formation	Sandstone, Mudstone
	Hunghae Formation	Sandstone, Mudstone
	Hakrim Formation	Sandstone, Mudstone
	Continental Sediments	Conglomerate
	~~ Unconformity ~~~	
Cretaceous	Volcanic rocks	Tuff
	Plutonic rocks	Granite

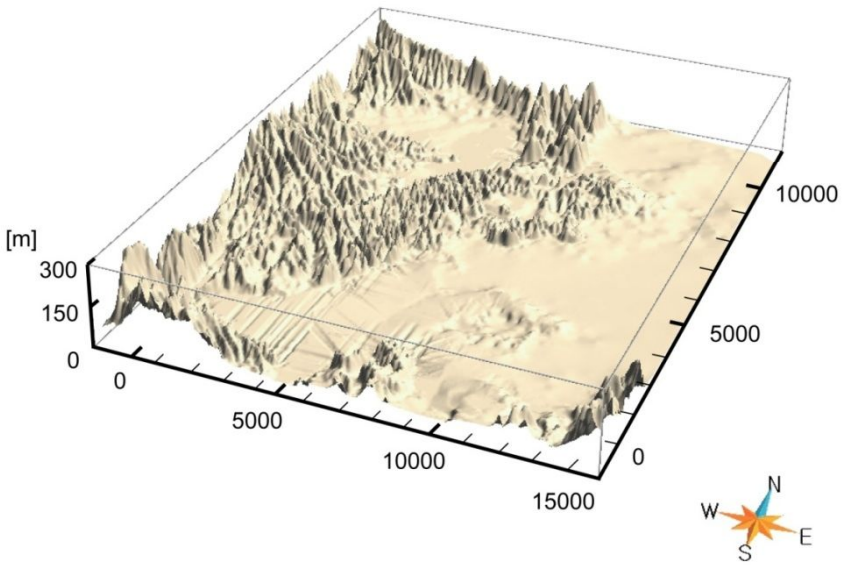

Figure 7. Digital elevation model of the Pohang Basin.

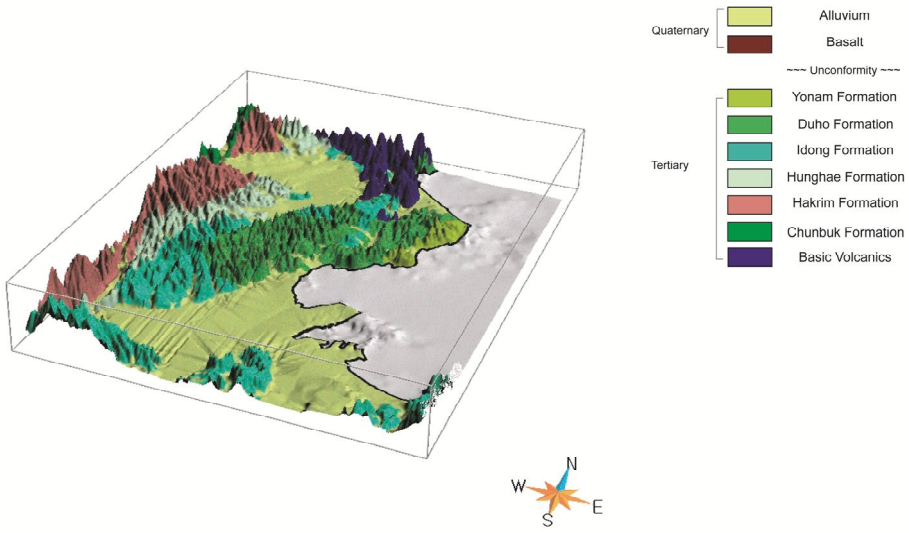

Figure 8. Digital elevation model with geologic map of the Pohang Basin.

surface, all geologic formation upper surfaces in modeling area are listed in Table 2. As shown in Table 2, each deep borehole data used in modeling does not include all geologic upper surfaces. The borehole PY-2, 301, B does not have boundary information of the plutonic and volcanic rocks, and A, C, PY-2, B does not have boundary information of the continental formation, and A, C, B, DS-1, DS-2 does not have boundary information of Hakrim Formation, and A, C, DS-1, DS-2 does not have boundary information of Hunghae and Idong Formation. Therefore, in this case, a series of geostatistical method such as an interpolation method is used in order to construct a geologic formation boundary surfaces in study area with no information. The interpolation algorithm used in this case is DSI algorithm. Each geologic formation upper surface established through DSI is shown in Fig. 9.

As a result of three-dimensional structural modeling, it is confirmed that the distribution of the plutonic rocks upper surface represent depth of 1174 ~ 1706 m (Fig. 10a), volcanic rocks upper surface represent depth of 408 ~ 941 m (Fig. 10b), tertiary continental sediments upper surface represent depth of 744 ~ 776 m (Fig. 10c), Hakrim Formation upper surface represent depth of 589 ~ 591 m (Fig. 10d), Heunghae Formation upper surface represent depth of 412 ~ 472 m (Fig. 11a), Idong Formation upper surface represent depth of 78 ~ 322 m (Fig. 11b), and Duho Formation upper surface represent depth of 31 ~ 50 m (Fig. 11c), and on top of those, upper surface of alluvium (Fig. 11d) is distributed.

Table 2. Borehole data with geologic formation upper surfaces used in this study.

Geologic formation upper surfaces	A [m]	C [m]	PY-2 [m]	301 [m]	302 [m]	DS-1 [m]	B [m]	DS-2 [m]
Duho Formation	50	50	34	47	47	50	50	50
Idong Formation	-	-	291	201	270	-	120	-
Hunghae Formation	-	-	460	430	440	-	760	-
Hakrim Formation	-	-	610	590	590	-	-	-
Continental Sediment	-	-	-	625	602	750	-	770
Volcanic rocks	424	436	-	-	-	822	875	843
Plutonic rocks	1182	1209	-	-	-	1409	1354	1518

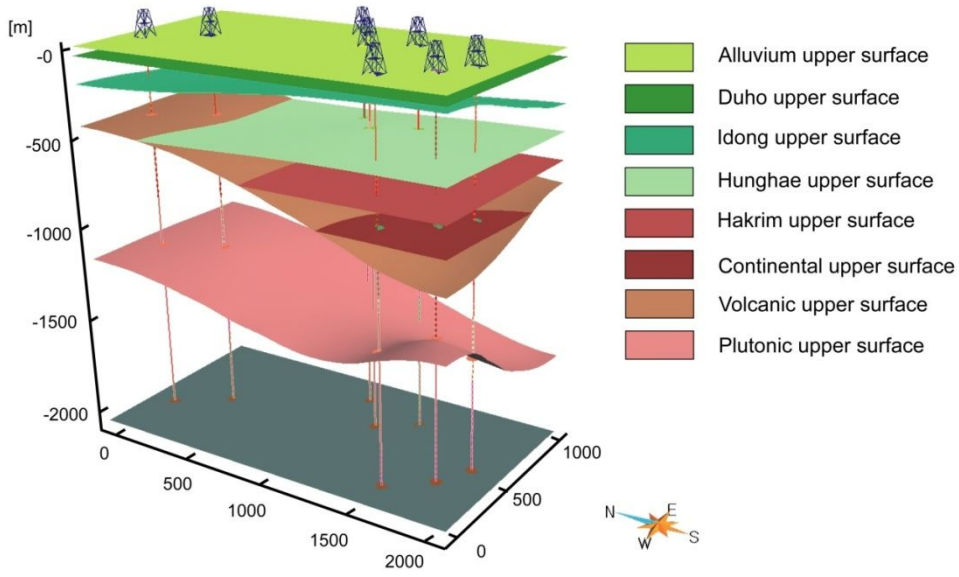

Figure 9. Three-dimensional structural model of the study area with 8 deep boreholes and 8 geologic formation upper surfaces.

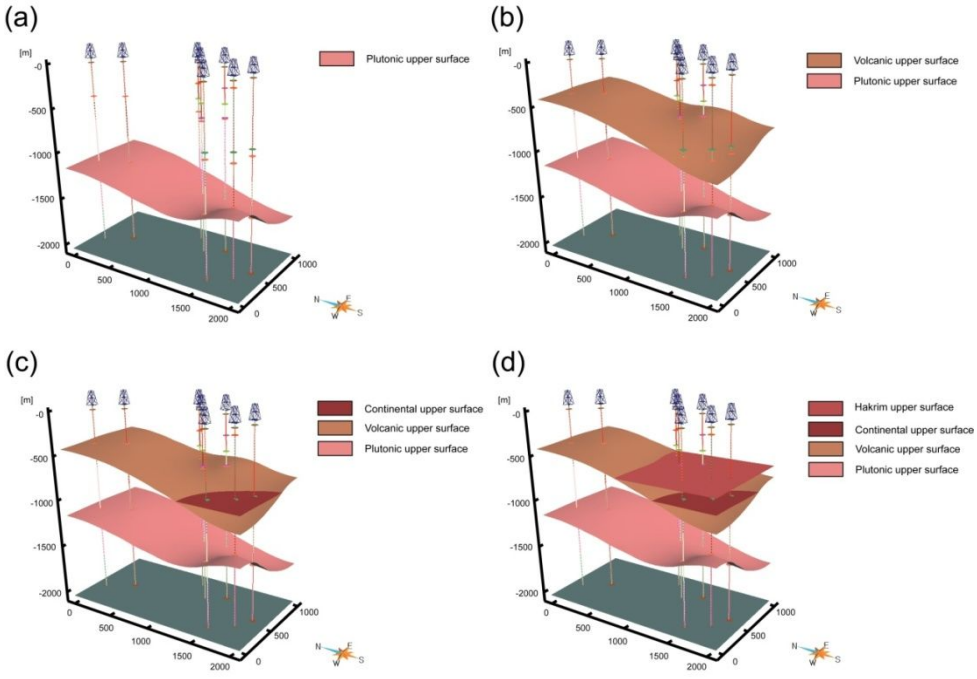

Figure 10. Geologic formation upper surfaces of the study area from bottom to top: (a) plutonic rockssupper surfaces, (b) volcanic rockssupper surfaces, (c) continental sediments upper surfaces, and (d) Hakrim Formation upper surfaces.

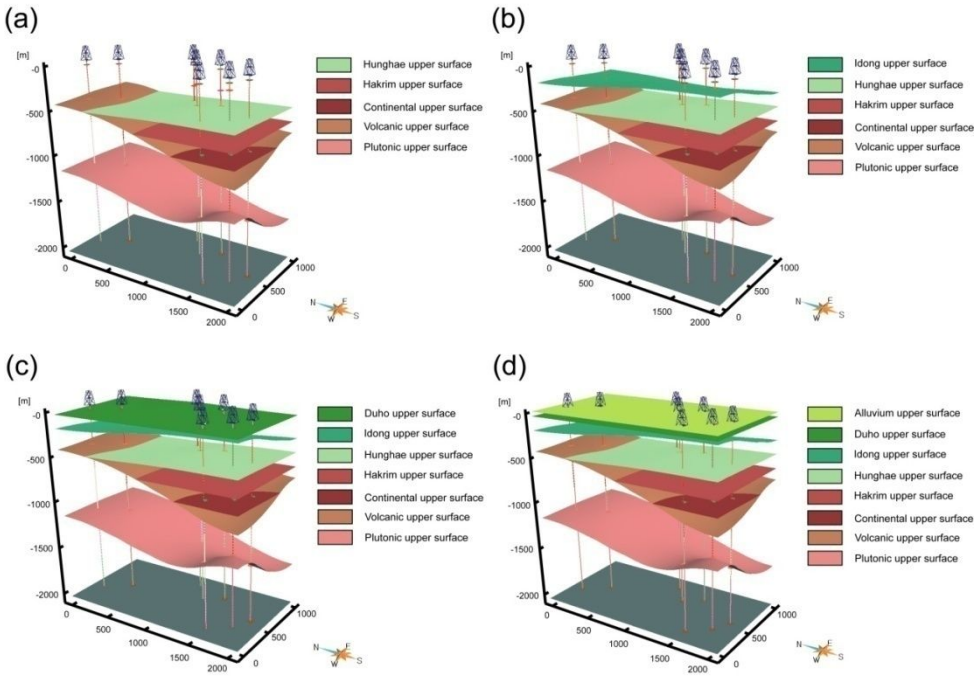

Figure 11. Geologic formation upper surfaces of the study area from bottom to top: (a) Hunghae Formation upper surfaces, (b) Idong Formation upper surfaces, (c) Duho Formation upper surfaces, and (d) alluvium upper surfaces.

4.3.2. Three-dimensional grid modeling

Three-dimensional grid model composed of three-dimensional grid with total 2,046,000 deformable cells is constructed (Fig.12). The deformable cells are formed by hexahedron, which is fitted to the geologic formation boundary surfaces of three-dimensional structural model. The generated three-dimensional grid model is composed of 60 cells in the east-west direction, 110 cells in the south-north direction and 310 layers. In addition, the model is composed of eight blocks separately because this model is based on nine geologic formation boundary surfaces established through three-dimensional structural modeling.

According to the result of three-dimensional grid model, especially, hexahedron cells are made finely around Hakrim and Heunghae Formation upper surface adjacent to volcanic rocks in three-dimensional structural model, and around area of narrowing down between Duho and Idong Formation upper surface as well.

4.3.3. Three-dimensional geologic formation modeling

Three-dimensional geologic formation modeling is performed by integrating three-dimensional structural model and three-dimensional grid model in order to establish three-dimensional geologic formation model representing geologic formation and geologic features of above mentioned study area. Established three-dimensional geologic formation model is shown in Fig. 13. In addition, Fig. 14 and Fig. 15 show that three-dimensional geologic formation model is distributed by order of the

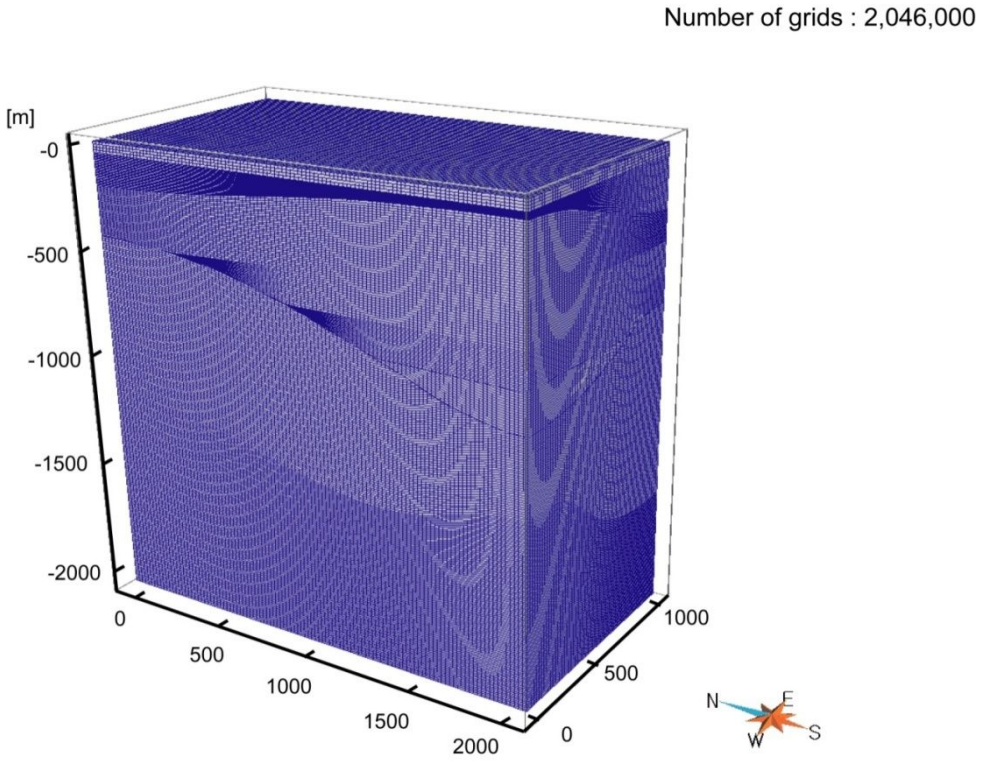

Figure 12. Three-dimensional grid model including three-dimensional grid with total 2,046,000 deformable cells formed by hexahedron.

cretaceous plutonic rocks (Fig.14a) and volcanic rocks (Fig. 14b), and tertiary continental sediments (Fig.14c) that covered by these base rocks, Hakrim (Fig.14d) and Heunghae (Fig.15a), Idong (Fig.15b), and Duho Formation (Fig.15c) corresponding to marine sediments, and quaternary alluvium (Fig.15d).

According to the result of three-dimensional geologic formation modeling, it is confirmed that the tertiary formations include the continental sediments and marine sediments but the tertiary formation is composed mostly of the marine sediments. In addition, these geologic formations are established finely in block type. Thus, number of cells, a volume, and a percentage of each geologic formation is analyzed quantitatively. The analyzed statistics values are summarized in Table3. As a result of the analysis, the plutonic rocks, volcanic rocks, continental sediments, Hakrim, Hunghae, Idong, Duho Formation, and alluvium are composed of 653,400, 620,400, 118,800, 118,800, 112,200, 211,200, 184,800, and 26,400 cells, respectively. Moreover, among eight geologic formations, a volume of the cretaceous plutonic rocks is 2.1793×10^9 m^3 of total 37.83% indicating the most distributed one. Especially, among the tertiary formations, a volume of Idong Formation corresponding to the Pohang Basin is the most distributed with 6.0369×10^8 m^3. On the other hand, a volume of the Hakrim Formation is the least distributed with 1.3463×10^8 m^3.

4.3.4. Three-dimensional lithofacies modeling

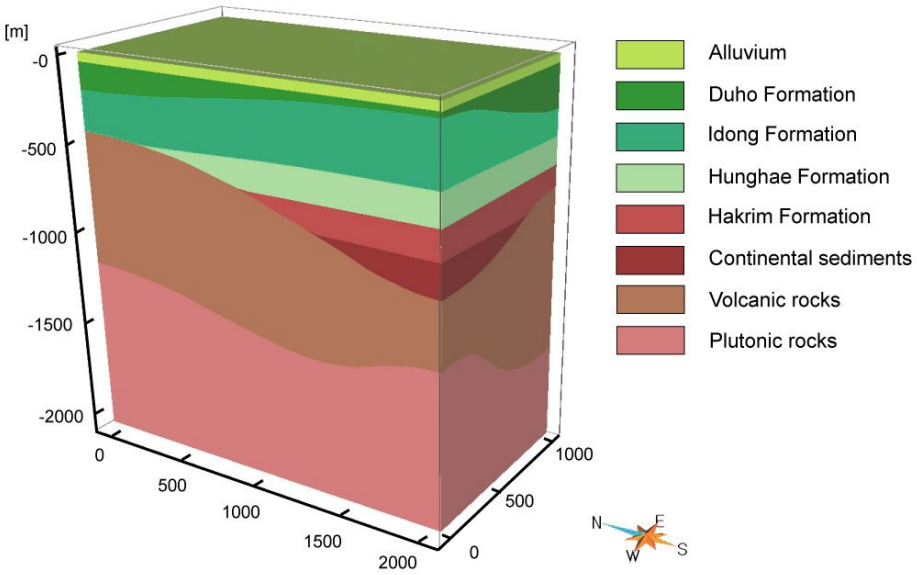

Figure 13. Three-dimensional geologic formation model of the Pohang Basin.

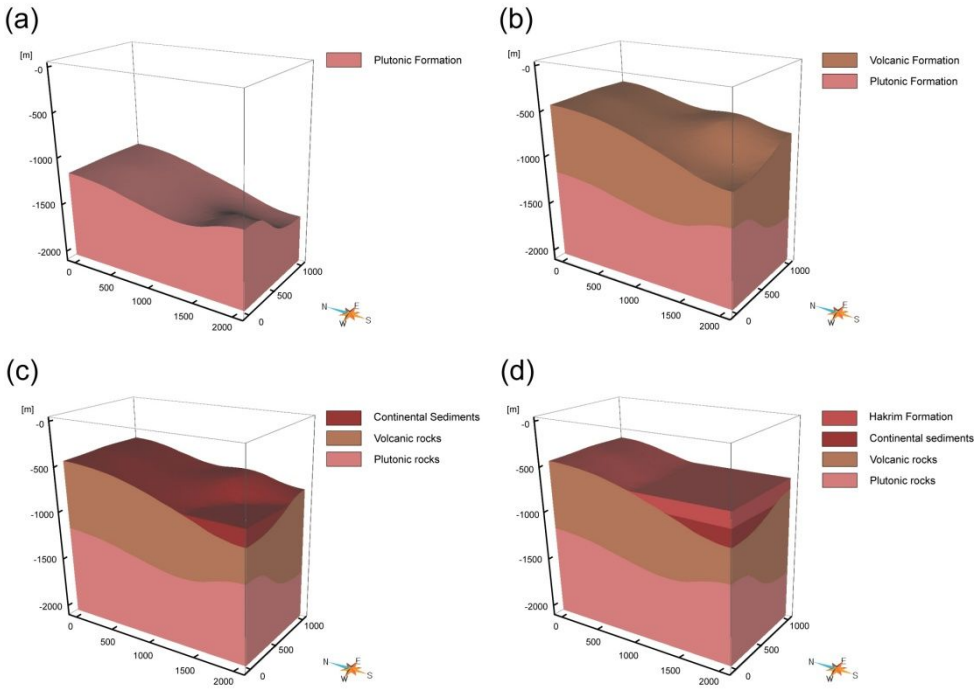

Figure 14. Three-dimensional geologic formation model of the Pohang Basin from bottom to top: (a) plutonic rocks, (b) volcanic rocks, (c) continental sediments, and (d) Hakrim Formation.

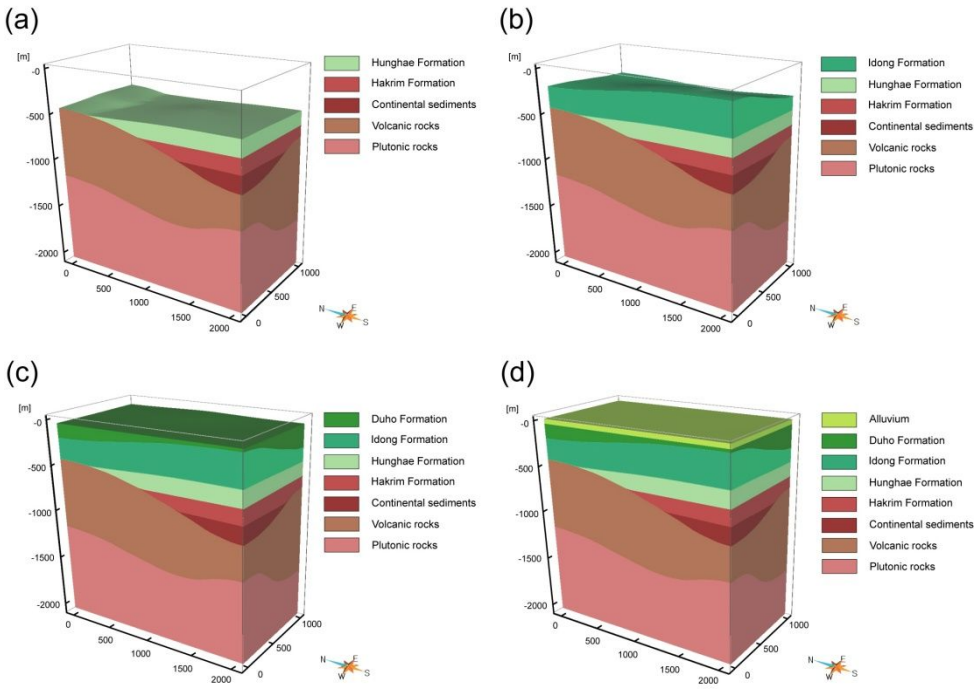

Figure 15. Three-dimensional geologic formation model of the Pohang Basin from bottom to top: (a) Hunghae Formation, (b) Idong Formation, (c) Duho Formation, and (d) alluvium.

Table 3. Statistical values of the grid, the volume and percentage in stratigraphic unit.

Stratigraphic unit	Number of cells	Volume [m^3]	Percentage [%]
Alluvium	26,400	1.2529×10^8	2.18
Duho Formation	184,800	4.2485×10^8	7.38
Idong Formation	211,200	6.0369×10^8	10.48
Hunghae Formation	112,200	2.7156×10^8	4.71
Hakrim Formation	112,200	1.3463×10^8	2.34
Continental Sediments	118,800	4.0169×10^7	0.70
Volcanic rocks	620,400	1.9806×10^9	34.38
Plutonic rocks	653,400	2.1793×10^9	37.83

Three-dimensional lithofacies modeling is performed in order to estimates and analyzes a distribution of lithofacies in uninvestigated area and used by only six deep boreholes (A, B, C, PY2, 301, 302) among eight deep boreholes (A, B, C, DS-1, DS-2, PY2, 301, 302) used in three-dimensional geologic modeling. That is because there is no information on lithofacies in deep borehole DS-1 and DS-2. Therefore, SIS and TGS are performed by using six deep boreholes (A, B, C, PY2, 301, 302) in100 times, respectively. In this case, since the cretaceous plutonic rocks, volcanic rocks, and tertiary continental sediments is composed of granite, tuff and conglomerate as single lithofacies, respectively. Thus, three-dimensional lithofacies modeling is performed only of the tertiary marine sediments including Hakrim, Heunghae, Duho and Idong Formation (Fig. 16).

Before conducting three-dimensional lithofacies modeling, statistical analysis regarding lithofacies in the tertiary marine sediments obtained from six deep boreholes is conducted. In the result, 96.40% of mudstone shows a lot more distribution compared with 3.60% of sandstone. In addition, since three-dimensional lithofacies modeling is performed based on the established three-dimensional grid model, it is essential that lithofacies information of raw data is modified by upscaling for a grid element. Therefore, in this study, upscaling method is used like blocking methods. The blocking method is used for gridding and upscaling raw data including lithofacies information of six deep boreholes (A, B, C, PY2, 301, 302). The used blocking methods are nearest to cell center, largest

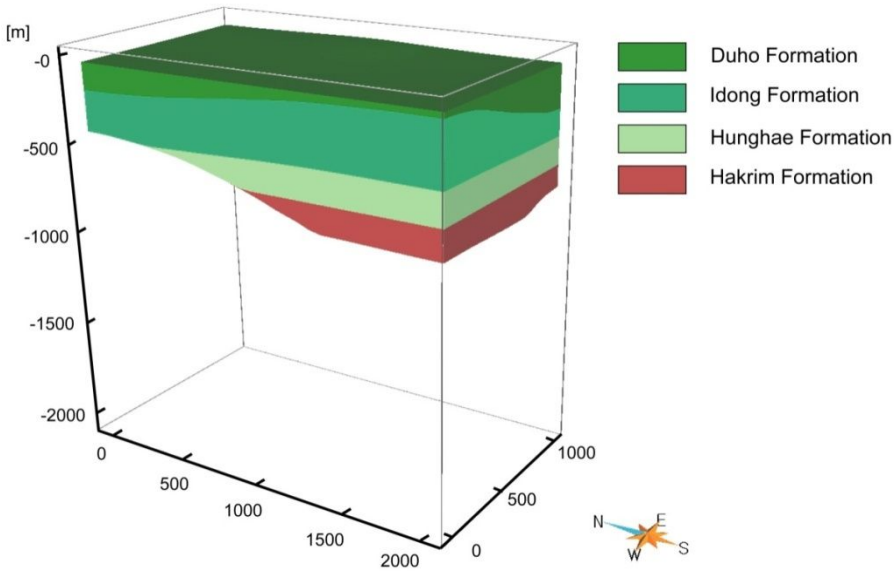

Figure 16. The tertiary marine sediments for three-dimensional lithofacies modeling in this study.

proportion and random method. As a result of blocking methods, among three blocking methods, nearest to cell center method is most similar to lithofacies proportion of the raw data with 96.60% of mudstone and 3.40% of sandstone. Fig.17 shows the results of the blocking methods. Then, three-dimensional lithofacies modeling is performed by applying the blocked data and the modeling results are as followings.

4.3.4.1 Varogram modeling

An experimental variogram values are calculated in order to calculate spatial correlation of six deep borehole data through variogram analysis explained above. In this study, the most common models that include the spherical, Gaussian and exponential model are used to determine an ideal theoretical variogram model among azimuth from 0° to 180° and dip from 0° to 90° at intervals of 30° of the calculated experimental variogram models. In addition, regression analysis is conducted such as sum of squares of regression error (SSR) and coefficient of determination (R^2) in order to determine an ideal theoretical variogram model also. In this analysis, the smaller a SSR value is, and the closer a R^2 value to 1.0 is variogram model that indicate ideal model. The analysis results are listed in Table 4.

According to the analysis results, the range is shortest at azimuth 150° and dip 90° with 118.7860 m, on the other hand, the range is longest at azimuth 180° and dip 0° with 363.6040 m.

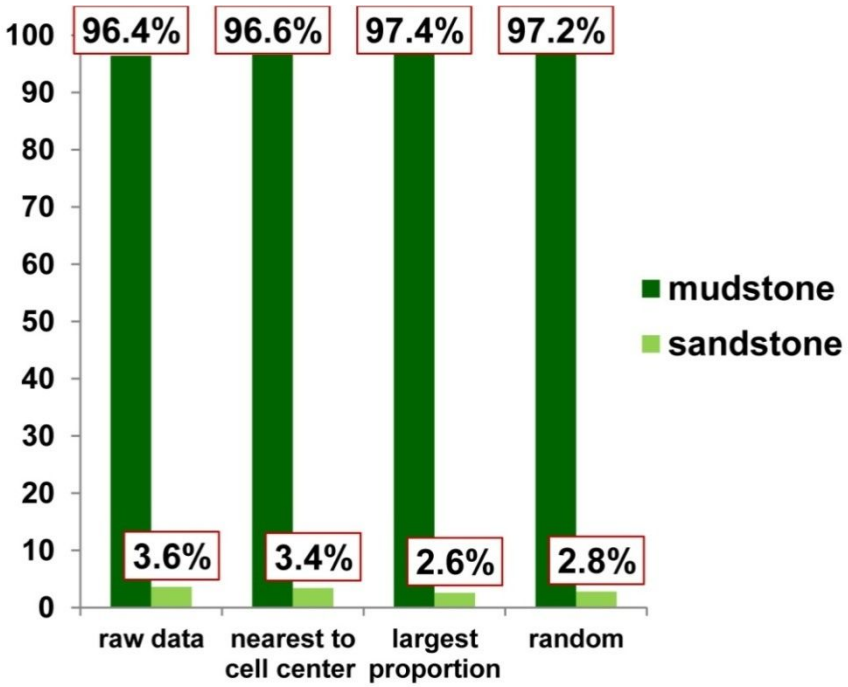

Figure 17. Bar chart of proportion between mudstone and sandstone for blocking methods.

Table 4. Variogram analysis for the lithofacies data.

Azimuth	Dip	Model								
		Spherical model			Gaussian model			Exponential model		
		Range [m]	SSR	R^2	Range [m]	SSR	R^2	Range [m]	SSR	R^2
0°	0°	356.5350	0.0074	0.4217	356.5350	0.0101	0.5769	356.5350	0.0055	0.3128
	30°	334.4280	0.0063	0.4708	334.4280	0.0088	0.6540	334.4280	0.0050	0.3744
	60°	332.6840	0.0063	0.4690	332.6840	0.0087	0.6512	332.6840	0.0045	0.3341
	90°	338.5660	0.0082	0.3870	338.5660	0.0109	0.5149	338.5660	0.0062	0.2922
30°	0°	347.4070	0.0083	0.4730	347.4070	0.0115	0.6517	347.4070	0.0061	0.3469
	30°	327.6750	0.0072	0.5409	327.6750	0.0101	0.7573	327.6750	0.0052	0.3886
	60°	327.0480	0.0073	0.5523	327.0480	0.0102	0.7702	327.0480	0.0053	0.3998
	90°	327.0480	0.0090	0.4224	327.0480	0.0120	0.5645	327.0480	0.0066	0.3110
60°	0°	327.6020	0.0078	0.4198	327.6020	0.0102	0.5464	327.6020	0.0059	0.3189
	30°	329.0980	0.0071	0.4214	329.0980	0.0094	0.5563	329.0980	0.0052	0.3068
	60°	328.1930	0.0105	0.4944	328.1930	0.0120	0.5673	328.1930	0.0072	0.3407
	90°	335.8730	0.0167	0.4560	335.8730	0.0198	0.5411	335.8730	0.0138	0.3771
90°	0°	350.0340	0.0069	0.5371	350.0340	0.0100	0.7698	350.0340	0.0052	0.4010
	30°	333.8600	0.0210	0.4540	333.8600	0.0239	0.5146	333.8600	0.0169	0.3643
	60°	333.6770	0.0205	0.4414	333.6770	0.0238	0.5136	333.6770	0.0168	0.3633
	90°	333.6770	0.0204	0.4459	333.6770	0.0238	0.5208	333.6770	0.0169	0.3697
120°	0°	334.4320	0.0064	0.4995	334.4320	0.0092	0.7187	334.4320	0.0046	0.3632
	30°	333.2550	0.0096	0.3240	333.2550	0.0129	0.4340	333.2550	0.0072	0.2430
	60°	333.0190	0.0201	0.4383	333.0190	0.0232	0.5073	333.0190	0.0162	0.3546
	90°	332.3600	0.0201	0.4384	332.3600	0.0230	0.5025	332.3600	0.0160	0.3494
150°	0°	130.6940	0.0202	0.3072	130.6940	0.0223	0.3393	130.6940	0.0198	0.3013
	30°	118.9300	0.0190	0.3311	118.9300	0.0207	0.3602	118.9300	0.0184	0.3200
	60°	119.9010	0.0236	0.3150	119.9010	0.0246	0.3287	119.9010	0.0222	0.2955
	90°	118.7860	0.0234	0.3119	118.7860	0.0246	0.3281	118.7860	0.0221	0.2951
180°	0°	363.6040	0.0042	0.5835	363.6040	0.0063	0.8624	363.6040	0.0031	0.4212
	30°	329.3600	0.0088	0.2552	329.3600	0.0108	0.3144	329.3600	0.0064	0.1849
	60°	328.5540	0.0094	0.2560	328.5540	0.0117	0.3209	328.5540	0.0072	0.1978
	90°	327.0140	0.0068	0.3129	327.0140	0.0090	0.4128	327.0140	0.0050	0.2307

In addition, the results of regression analysis show that the SSR value is smallest at azimuth 180° and dip 0° of exponential model with 0.0031, on the other hand, the SSR value is largest at azimuth 150° and dip 60° of spherical model with 0.0246. Moreover, the R^2 value is smallest at azimuth 180° and dip 30° of exponential model with 0.1849; on the other hand, the R^2 value is closest to 1 at azimuth 180° and dip 0° of Gaussian model with 0.8624. Accordingly, the experimental variogram and the theoretical variogram at azimuth 180° and dip 0° show that has a good spatial correlation (Fig. 18). Besides, as a result of the regression analysis, it is confirmed that ideal theoretical variogram model is at azimuth 180° and dip 0° of Gaussian model among the three models (Fig.19.) and it is summarized in Table 5. Also, Fig.20 shows a schematic of the determined ideal theoretical variogram at study area.

4.3.4.2 Results of conditional simulation

For lithofacies estimation of uninvestigated area, SIS is performed by applying mentioned the determined theoretical variogram in 100 times. The Fig.21a, b and c is the first, fiftieth and hundredth result of SIS among 100 times realization results. It is confirmed that the distribution of mudstone is distributed remarkably much more in comparison to the distribution of sandstone. The result means that lithofacies information of raw data is well reflected. Meanwhile, there are some difficulties in figuring out directivity and continuity of predicted lithofacies distributions

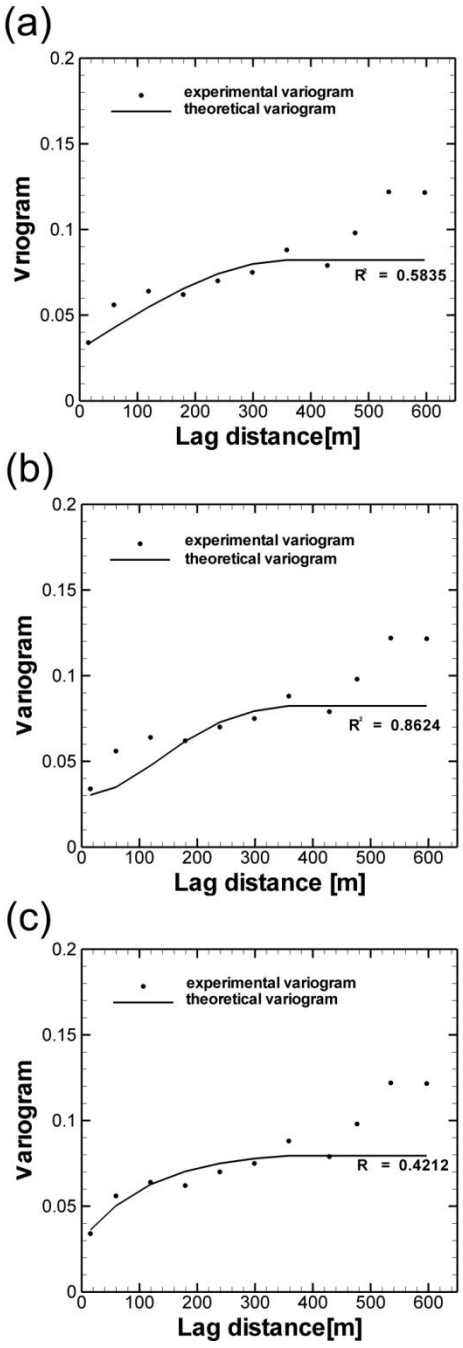

Figure 18. Experimental variogram and theoretical variogram at azimuth 180° and dip 0° for the field data: (a) spherical model, (b) Gaussian model, and (c) exponential model.

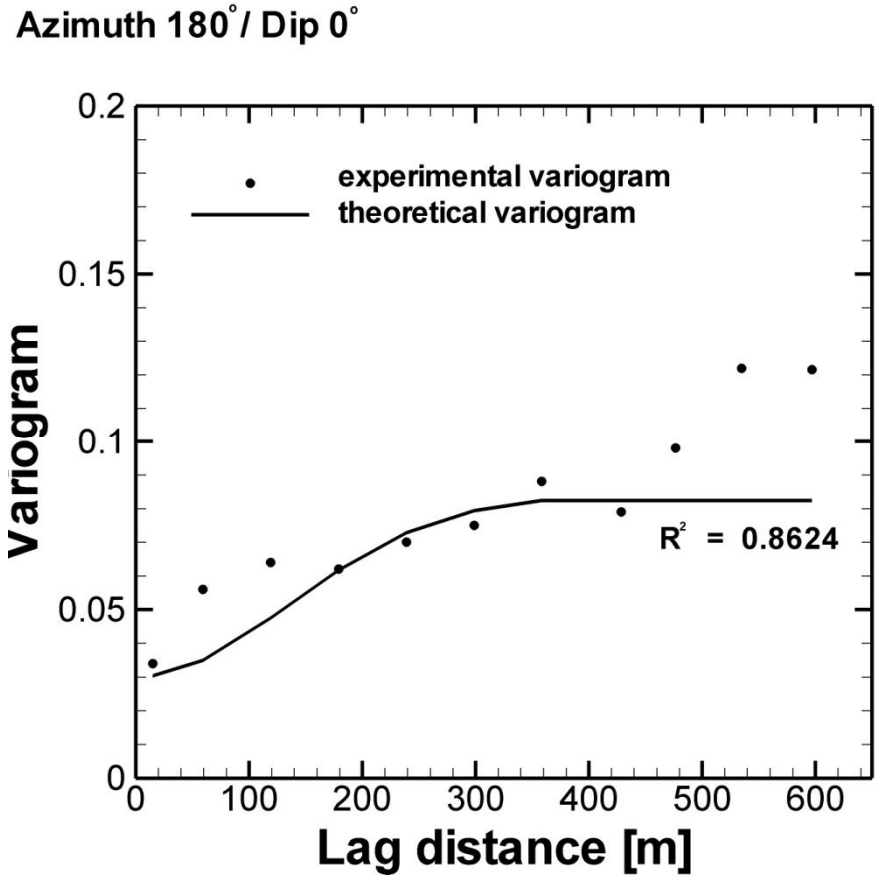

Figure 19. Experimental variogram and theoretical variogram of Gaussian model with azimuth of 180° and dip of 0° used in three-dimensional lithofacies modeling.

Table 5. Ideal theoretical variogram model for the lithofacies data.

Azimuth	Dip	Gaussian model				
		sill	nugget	Range[m]	SSR	R^2
180°	0°	0.0822	0.0300	363.6040	0.0063	0.8624

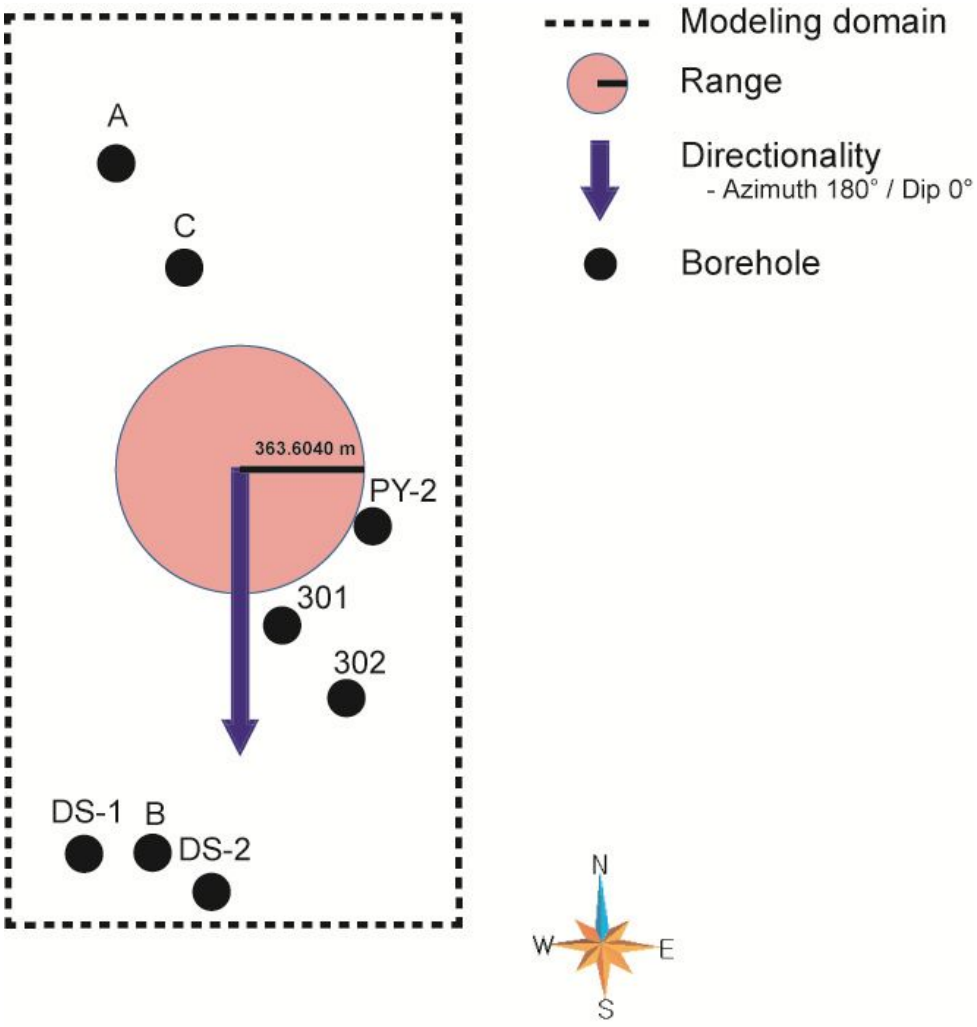

Figure 20. Schematic diagram of the determined ideal theoretical variogram at study area.

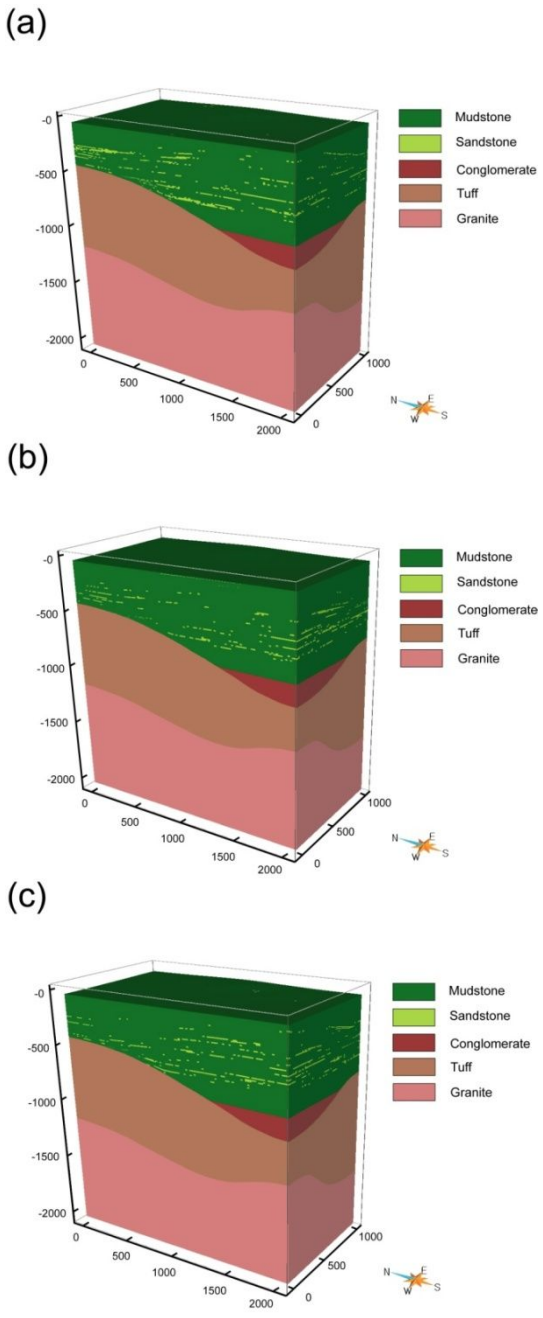

Figure 21. Three-dimensional lithofacies model with (a) the first, (b) the fiftieth, and (c) the hundredth result of SIS among 100 times realization results.

from this result. Therefore, analysis of SIS for sandstone except mudstone is conducted in order to figure out directivity and continuity of predicted lithofacies distribution and the Fig. 22 shows the result of the first (Fig.22a), the fiftieth (Fig.22b), and the hundredth (Fig.22c) among 100 times realization results. According to the results, it is confirmed that sandstone mainly distributes disorderly and discursively showing horizontal direction extensity rather than vertical direction in entire modeling area. For TGS, 100 times realization is performed by applying above-mentioned the ideal theoretical variogram. The Fig.23a, b and c is the first, the fiftieth and the hundredth result of TGS among 100 times realization results. Like SIS, in regards to sandstone except mudstone, analysis of TGS is conducted and the Fig. 24 shows the result of the first (Fig.24a), the fiftieth (Fig.24b), and the hundredth (Fig.24c) among 100 times realization results.

The Fig. 25, 26 and 27 is the first, the fiftieth and the hundredth result of SIS and TGS among 100 times realization results for sandstone. As shown in the Fig.25, 26 and 27, three-dimensional lithofacies model result using TGS shows that sandstone is distributed in relatively smaller ratio compared with the result from SIS, and is distributed around the borehole data location showing horizontal direction extensity rather than vertical direction. Due to stochastic characters, SIS and TGS have different results of each simulation all the time. According to the stochastic characters, the statistical analyses of 100 times simulations are performed for mean value, standard deviation, maximum value, and minimum value of an estimated

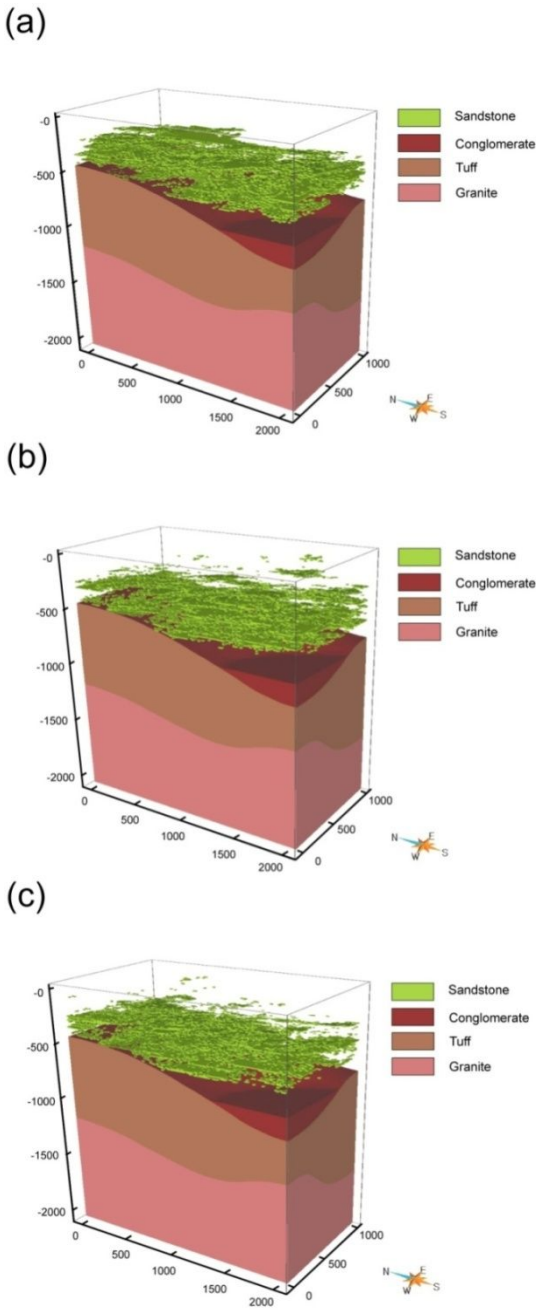

Figure 22. Three-dimensional lithofacies model for sandstone with (a) the first, (b) the fiftieth, and (c) the hundredth result of SIS among 100 times realization results.

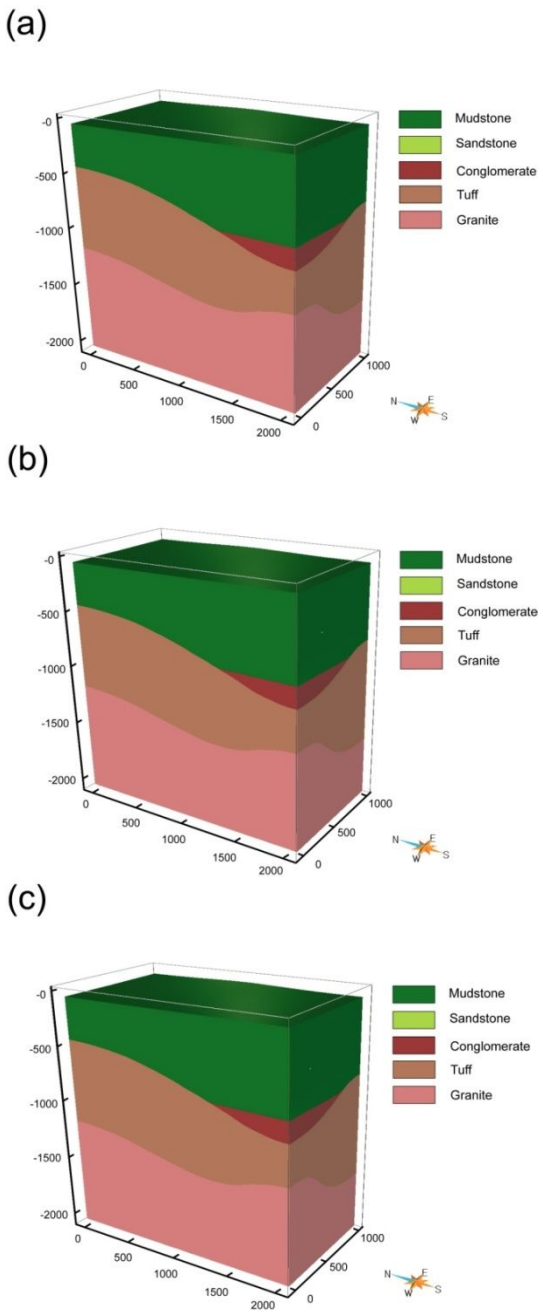

Figure 23. Three-dimensional lithofacies model with (a) the first, (b) the fiftieth, and (c) the hundredth result of TGS among 100 times realization results.

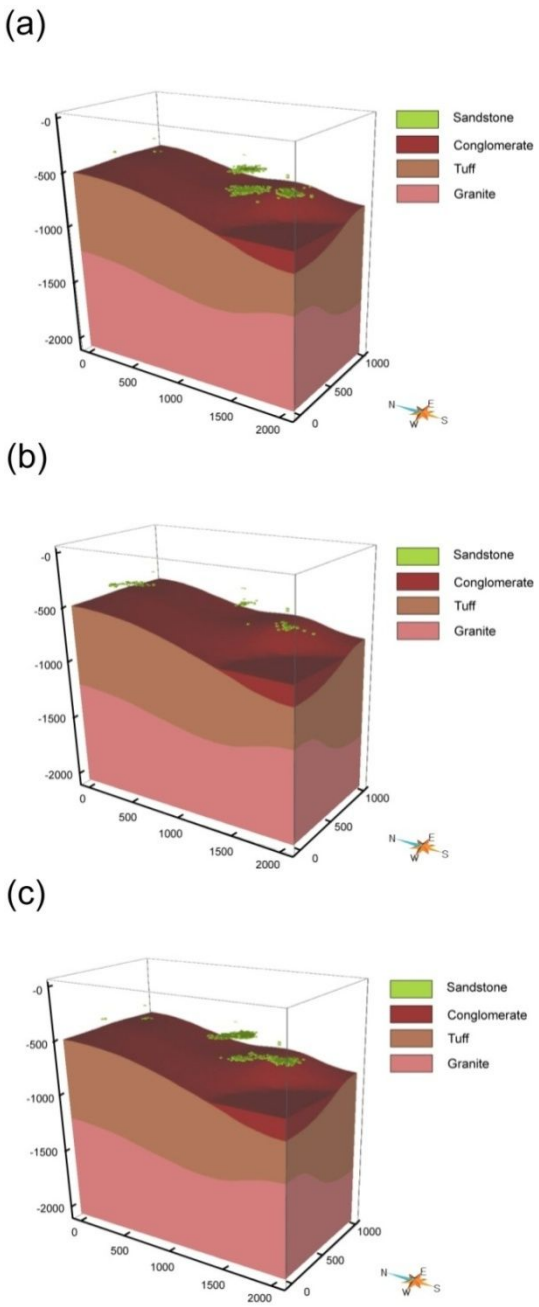

Figure 24. Three-dimensional lithofacies model for sandstone with (a) the first, (b) the fiftieth, and (c) the hundredth result of TGS among 100 times realization results.

(a)

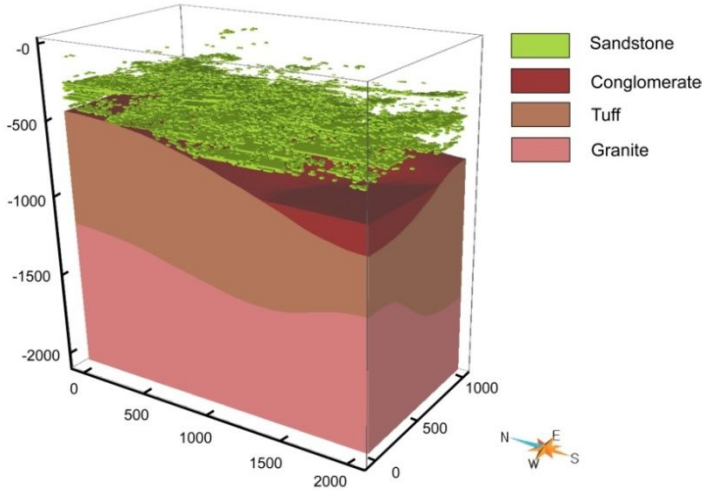

(b)

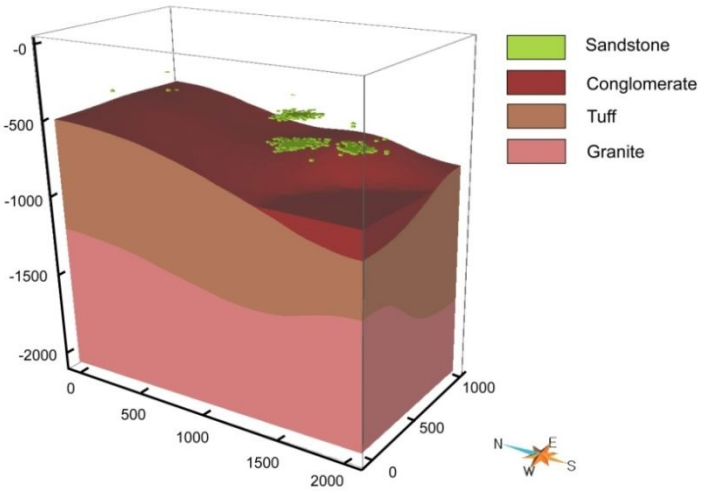

Figure 25. Three-dimensional lithofacies model of (a) SIS and (b) TGS result with the first among 100 times realization results.

(a)

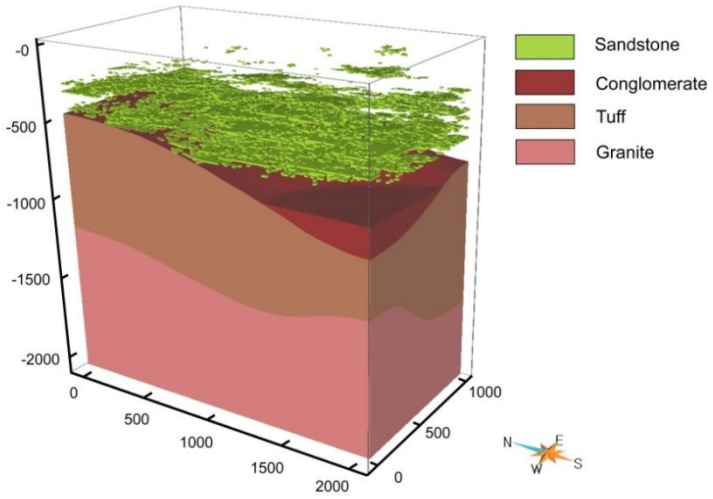

(b)

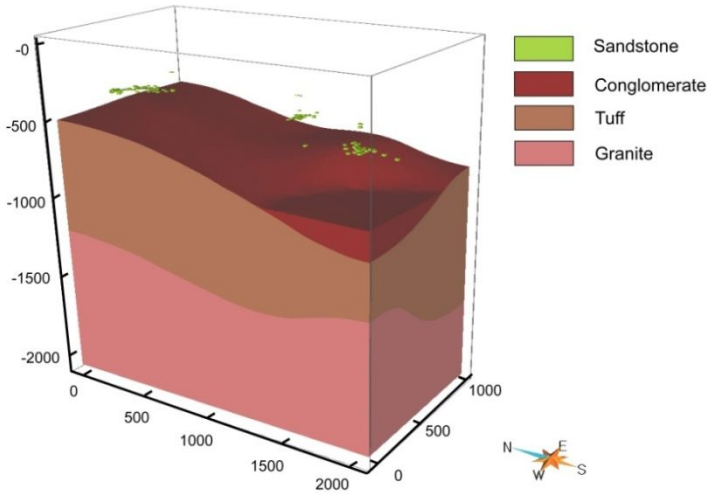

Figure 26. Three-dimensional lithofacies model of (a) SIS and (b) TGS result with the fiftieth among 100 times realization results.

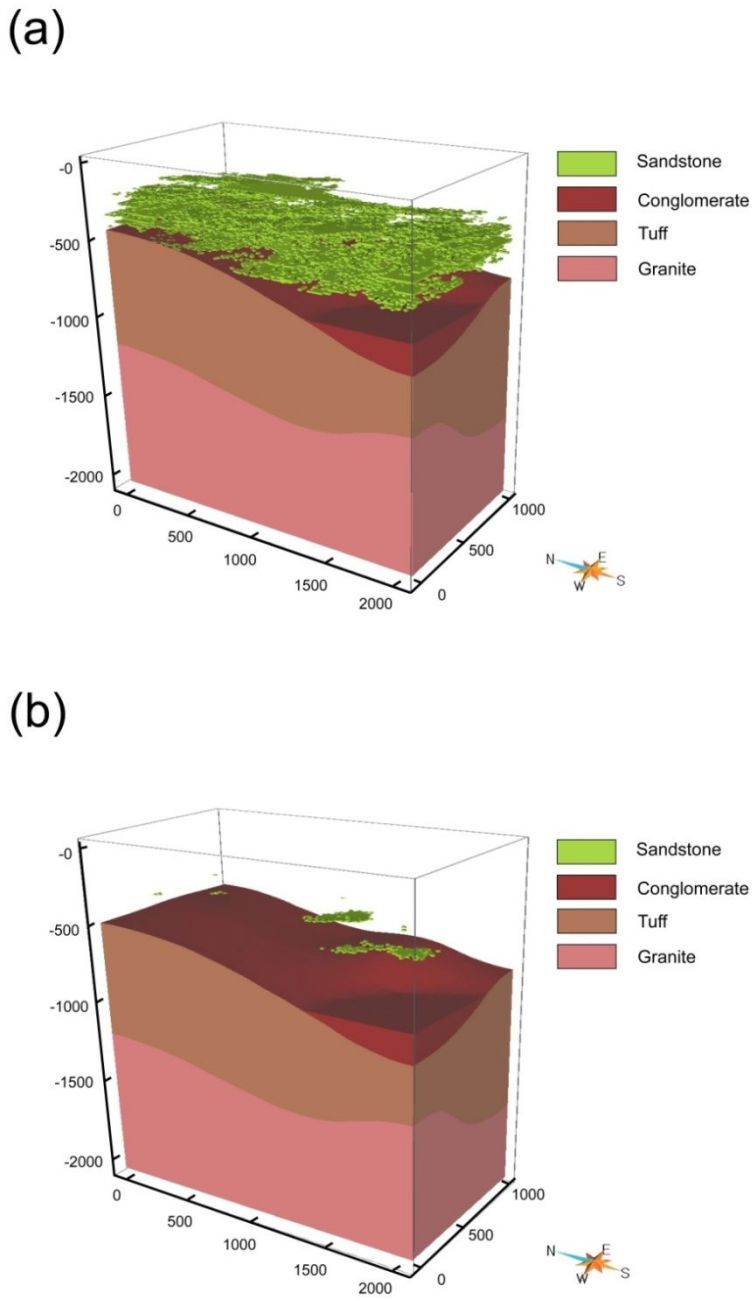

Figure 27. Three-dimensional lithofacies model of (a) SIS and (b) TGS result with the hundredth among 100 times realization results.

volume of mudstone and sandstone. The statistical values are listed in Table 6. The statistical analysis result of Table 6 is illustrated in Fig. 28 and Fig. 29.

As a result of SIS, the volume of mudstone and sandstone shows the range of $1.3556 \times 10^9 \sim 1.3932 \times 10^9$ m^3 and $4.2071 \times 10^7 \sim 7.9092 \times 10^7$ m^3, respectively. As far as mean value is concerned, mudstone is dominating over sandstone with 1.3734×10^9 and 6.1336×10^6 m^3, respectively. As a result of TGS, the volume of mudstone and sandstone shows the range of $1.4329 \times 10^9 \sim 1.4346 \times 10^9$ m^3 and $1.5029 \times 10^5 \sim 1.8485 \times 10^6$ m^3, respectively. As far as mean value is concerned, mudstone is dominating over sandstone with $1.4341 \times 10^9$and 6.3964×10^5 m^3, respectively. Meanwhile, mudstone ratio from TGS shows relatively small ratio compared with SIS result. In addition, Fig.30 shows that a mudstone and sandstone ratio of SIS is 95.48% and 4.52%, respectively. Thus, the ratios are similar to raw data of 96.40% and 3.60% in results, respectively. On the contrary, a mudstone and sandstone ratio of TGS is 99.68% and 0.32%, respectively. Thus, the ratios are different to the ratio of raw data.

5. Cross-validation

The ultimate approach of cross-validation is to assess the quality of the estimated data by comparing with raw data. In this study, three-dimensional lithoface is modeling for cross-validation is performed using

Table 6. Statistical values of three-dimensional lithofacies modeling.

Algorithm	Statistical value	Mudstone [m^3]	Sandstone [m^3]
SIS	Minimum	1.3556×10^9	4.2071×10^7
	25th percentile	1.3688×10^9	5.6579×10^7
	Median	1.3737×10^9	6.0628×10^7
	75th percentile	1.3781×10^9	6.5718×10^7
	Maximum	1.3932×10^9	7.9092×10^7
	Mean	1.3734×10^9	6.1336×10^7
	Standard deviation	6.9845×10^6	6.9839×10^6
TGS	Minimum	1.4329×10^9	1.5029×10^5
	25th percentile	1.4339×10^9	3.5939×10^5
	Median	1.4342×10^9	5.3893×10^5
	75th percentile	1.4343×10^9	8.4941×10^5
	Maximum	1.4346×10^9	1.8485×10^6
	Mean	1.4341×10^9	6.3964×10^5
	Standard deviation	6.0180×10^5	6.0191×10^5

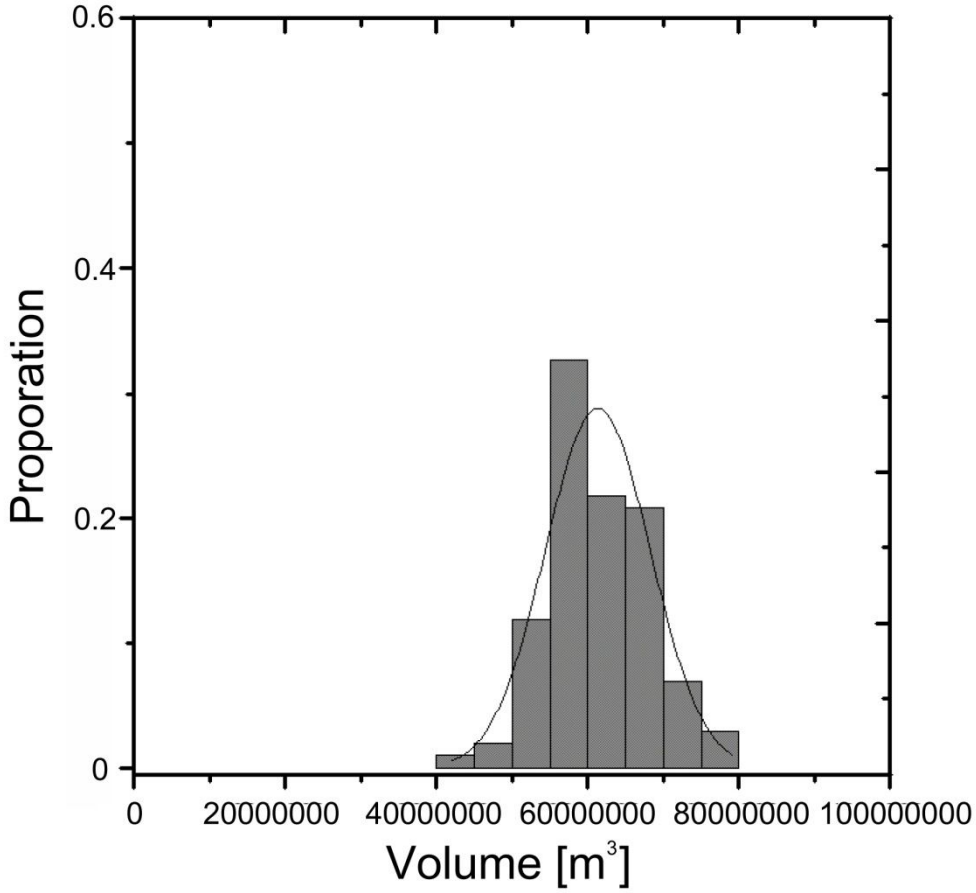

Figure 28. Histogram of the volume simulated using SIS for sandstone.

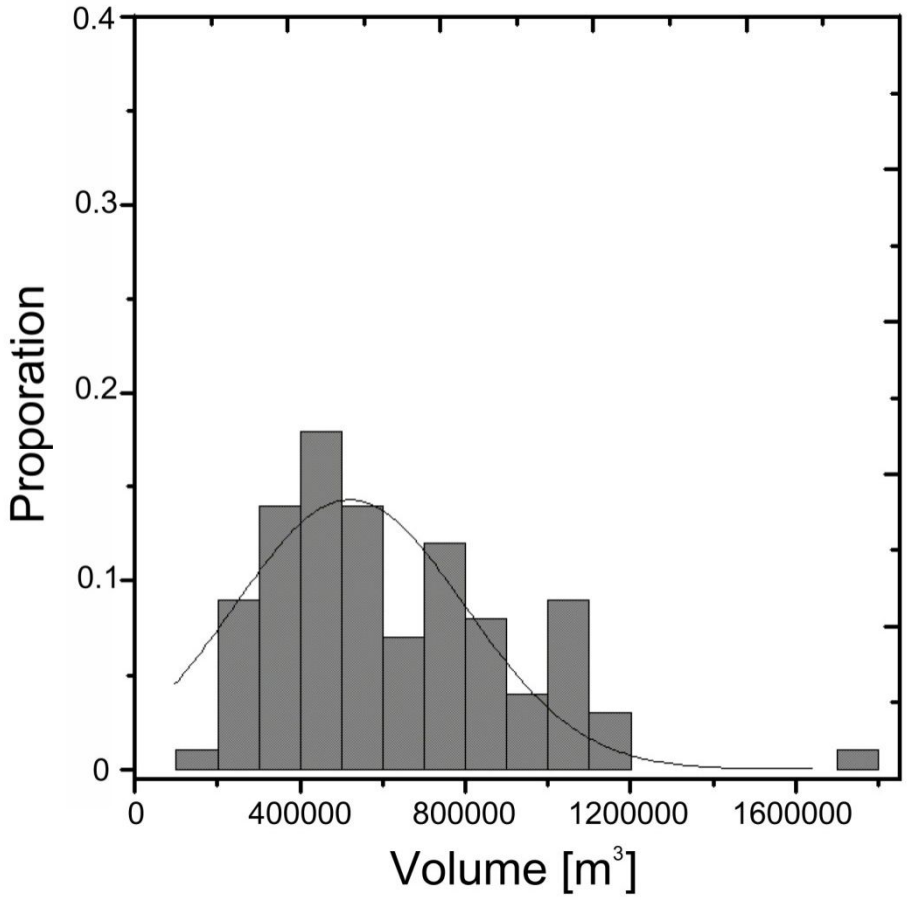

Figure 29. Histogram of the volume simulated using TGS for sandstone.

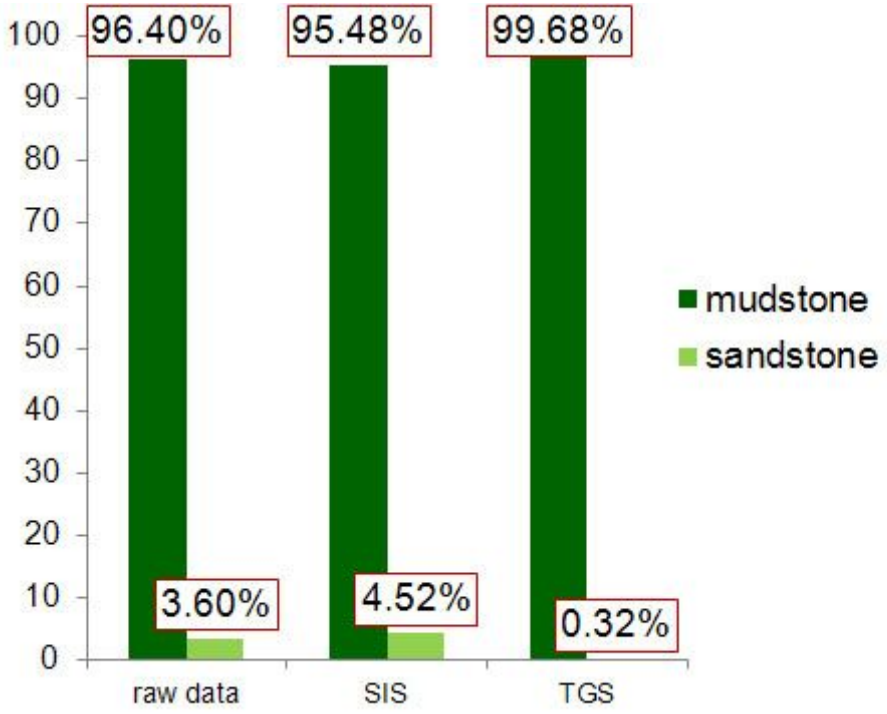

Figure 30. Bar chart of proportion between mudstone and sandstone for raw data, SIS, and TGS.

the five boreholes among the six boreholes (A, B, C, PY-2, 301, 302) and a compare and analyze with raw data are performed in order to identify a borehole that has a high level of dependence in lithofacies. In addition, regarding sandstone except mudstone, 100 times SIS and TGS are performed. The results of cross-validation for Case S-1 to S-6 of SIS and Case T-1 to T-6 of TGS are plotted in Fig.31 and Fig.32, respectively. The results are summarized in Table7.

Three-dimensional lithofacies modeling for Case S-1 is performed by using the five boreholes B, C, PY-2, 301 and 302 (Fig.31a). The result of Case S-1 shows that the volume of sandstone is included with the range of $4.6000 \times 10^7 \sim 7.9800 \times 10^7$ m^3 and the median and mean value are 6.0576×10^7 and 6.0265×10^7 m^3, respectively.

Three-dimensional lithofacies modeling for Case S-2 is performed by using the five boreholes A, C, PY-2, 301 and 302 (Fig.31b). The result of Case S-2 shows that the volume of sandstone is included with the range of $2.1000 \times 10^6 \sim 8.7500 \times 10^7$ m^3 and the median and mean value are 6.3268×10^7 and 6.3792×10^7 m^3, respectively.

Three-dimensional lithofacies modeling for Case S-3 is performed by using the five boreholes A, B, PY-2, 301 and 302 (Fig.31c). The result of Case S-3 shows that the volume of sandstone is included with the range of $4.3000 \times 10^7 \sim 7.3500 \times 10^7$ m^3 and the median and mean value are 5.7068×10^7 and 5.7216×10^7 m^3, respectively.

Three-dimensional lithofacies modeling for Case S-4 is performed by

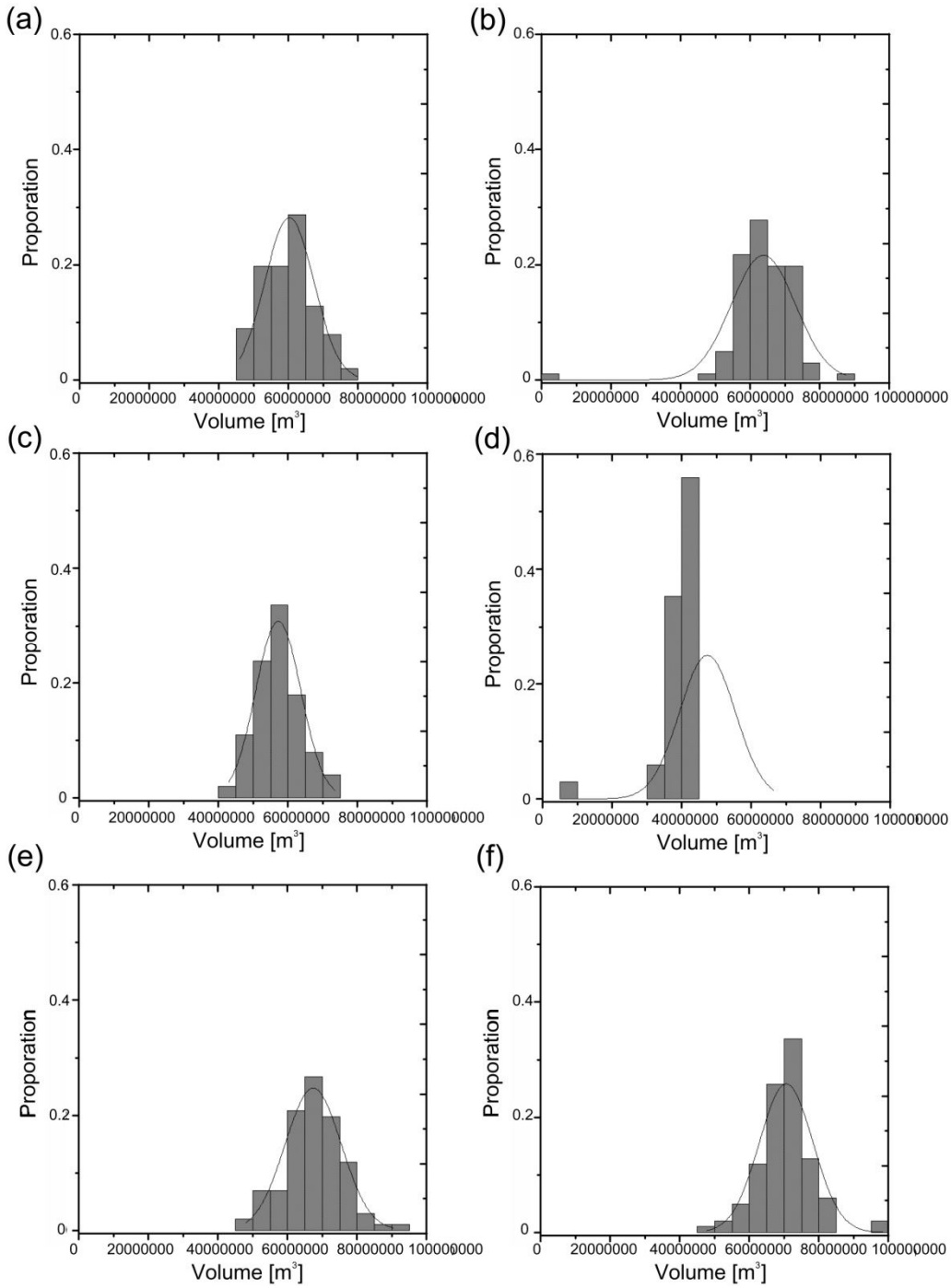

Figure 31. Histogram of the volume simulated using SIS for cross-validation: (a) Case S-1, (b) Case S-2 (c) Case S-3, (d) Case S-4, (e) Case S-5, and (f) Case S-6.

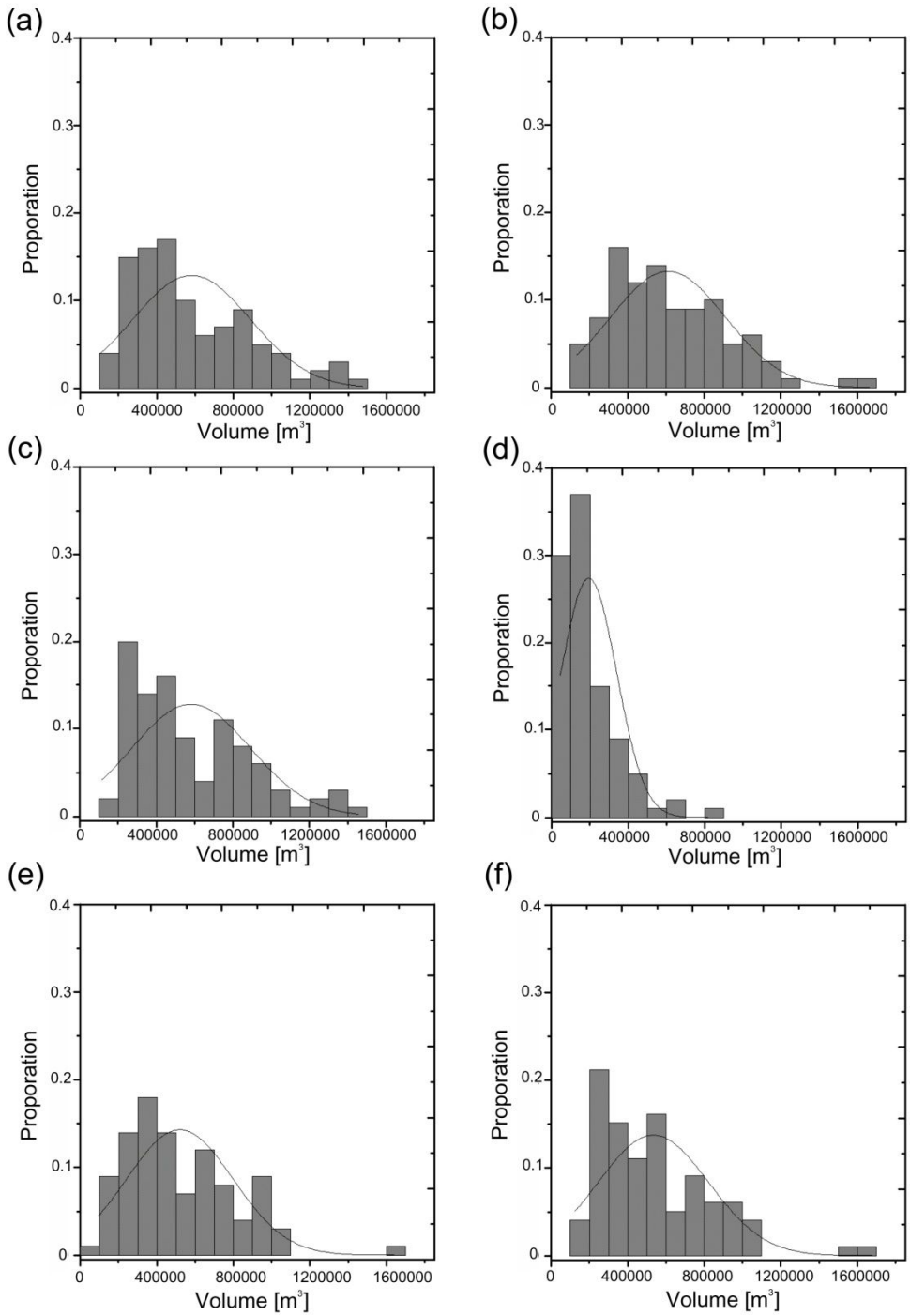

Figure 32. Histogram of the volume simulated using TGS for cross-validation: (a) Case T-1, (b) Case T-2 (c) Case T-3, (d) Case T-4, (e) Case T-5, and (f) Case T-6.

Table 7. Statistical values of three-dimensional lithofacies modeling for cross-validation.

Algorithm	Volume of sandstone [m^3]				
	Minimum	Maximum	Median	Mean	Standard deviation
SIS					
Case S-1	4.6000×10^7	7.9800×10^7	6.0576×10^7	6.0265×10^7	7.1522×10^6
Case S-2	2.1000×10^6	8.7500×10^7	6.3268×10^7	6.3792×10^7	9.3155×10^6
Case S-3	4.3000×10^7	7.3500×10^7	5.7068×10^7	5.7216×10^7	6.5337×10^6
Case S-4	6.5500×10^6	6.6500×10^7	4.7516×10^7	4.7384×10^7	8.1026×10^6
Case S-5	4.8100×10^7	9.0400×10^7	6.7399×10^7	6.7399×10^7	8.1507×10^6
Case S-6	4.7800×10^7	9.9900×10^7	7.0789×10^7	7.0617×10^7	7.8092×10^6
TSG					
Case T-1	1.0896×10^5	1.4800×10^6	4.8085×10^5	5.8134×10^5	3.1140×10^5
Case T-2	1.3453×10^5	1.6600×10^6	5.3688×10^5	6.1042×10^5	3.0148×10^5
Case T-3	1.1391×10^5	1.4600×10^6	4.8072×10^5	5.8154×10^5	3.1331×10^5
Case T-4	4.4461×10^4	8.3071×10^5	1.5650×10^5	1.9349×10^5	1.4632×10^5
Case T-5	9.6160×10^4	1.6400×10^6	4.5221×10^5	5.1973×10^5	2.8022×10^5
Case T-6	1.2535×10^5	1.6800×10^6	4.9069×10^5	5.3812×10^5	2.9341×10^5

using the five boreholes A, B, C, 301 and 302 (Fig.31d). The result of Case S-4 shows that the volume of sandstone is included with the range of $6.5500 \times 10^6 \sim 4.7516 \times 10^7$ $m^3$and the median and mean value are 6.6500×10^7 and 4.7384×10^7 m^3, respectively.

Three-dimensional lithofacies modeling for Case S-5 is performed by using the five boreholes A, B, C, PY-2 and 302 (Fig.31e). The result of Case S-5 shows that the volume of sandstone is included with the range of $4.8100 \times 10^7 \sim 9.0400 \times 10^7$ m^3 and the median and mean value are 6.7399×10^7 and 6.7399×10^7 m^3, respectively.

Three-dimensional lithofacies modeling for Case S-6 is performed by using the five boreholes A, B, C, PY-2, and 301 (Fig.31f). The result of Case S-6 shows that the volume of sandstone is included with the range of $4.7800 \times 10^7 \sim 9.9900 \times 10^7$ m^3 and the median and mean value are 7.0789×10^7 and 7.0617×10^7 m^3, respectively.

Three-dimensional lithofacies modeling for Case T-1is performed by using the five boreholes B, C, PY-2, 301 and 302 (Fig.32a). The result of Case T-1 shows that the volume of sandstone is included with the range of $1.0896 \times 10^5 \sim 1.4800 \times 10^6$ m^3 and the median and mean value are 4.8085×10^5 and 5.8134×10^5 m^3, respectively.

Three-dimensional lithofacies modeling for Case T-2 is performed by using the five boreholes A, C, PY-2, 301 and 302 (Fig.32b). The result of Case T-2 shows that the volume of sandstone is included with the range of $1.3453 \times 10^5 \sim 1.6600 \times 10^6$ m^3 and the median and mean value are

5.3688×10^5 and 6.1042×10^5 m^3, respectively.

Three-dimensional lithofacies modeling for Case T-3 is performed by using the five boreholes A, B, PY-2, 301 and 302 (Fig.32c). The result of Case T-3 shows that the volume of sandstone is included with the range of $1.1391 \times 10^5 \sim 1.4600 \times 10^6$ m^3 and the median and mean value are 4.8072×10^5 and 5.8154×10^5 m^3, respectively.

Three-dimensional lithofacies modeling for Case T-4 is performed by using the five boreholes A, B, C, 301, and 302 (Fig.32d). The result of Case T-4 shows that the volume of sandstone is included with the range of $4.4446 \times 10^4 \sim 8.3071 \times 10^5$ m^3 and the median and mean value are 1.5650×10^5 and 1.9349×10^5 m^3, respectively.

Three-dimensional lithofacies modeling for Case T-5 is performed by using the five boreholes A, B, C, PY-2, and 302 (Fig.32e). The result of Case T-5 shows that the volume of sandstone is included with the range of $9.6160 \times 10^4 \sim 1.6400 \times 10^6$ m^3 and the median and mean value are 4.5221×10^5 and 5.1973×10^5 m^3, respectively.

Three-dimensional lithofacies modeling for Case T-6 is performed by using the five boreholes A, B, C, PY-2, and 301 (Fig.32f). The result of Case T-6 shows that the volume of sandstone is included with the range of $1.2535 \times 10^5 \sim 1.6800 \times 10^6$ m^3 and the median and mean value are 4.9069×10^5 and 5.3812×10^5 m^3, respectively.

As a result of cross-validation for Case S-1 to S-6 of SIS, the volume of sandstone for Case S-2 show the widest range of $2.1000 \times 10^5 \sim$

8.7500×10^5 m^3 and the mean value of the volume of sandstone for Case S-1 show that the value is most similar to three-dimensional lithofacies model of SIS performed by using the six boreholes. On the order hand, Case S-4 shows the largest difference. In addition, As a result of cross-validation for Case T-1 to T-6 of TGS, the volume of sandstone for Case T-5 show the widest range of $9.6160 \times 10^4 \sim 1.6400 \times 10^6$ m^3 and the mean value of the volume of sandstone for Case T-2 show that is most similar to the volume of sandstone for three-dimensional lithofacies is model of SIS performed by using the six boreholes. On the order hand, Case T-4 shows the largest difference.

According to the results, Case S-4 and T-4 performed by using the five boreholes A, B, C, 301, and 302 show the largest difference from three-dimensional lithofacies model of SIS and TGS performed by using the six boreholes. Thus, the borehole PY-2 excluded from Case S-4 and Case T-4 indicate the highest level of dependence for three-dimensional lithofacies modeling in this study.

6. Conclusions

Three-dimensional geologic modeling is performed for quantitative characterization and realistic visualization about in the Pohang Basin, Korea in this study. First, GIS and borehole data are utilized and then three-dimensional structure, grid, geologic formation, and lithofacies modeling are performed next. Finally, cross-validation is performed.

Three-dimensional structural modeling is performed by using the DIS algorithm in order to construct the complex stratigraphic analysis, geologic structure analysis, and others in study area. As a result, it is confirmed that the distribution of stratigraphic boundary in study area. The confirmed stratigraphic boundaries are the cretaceous plutonic rocks, volcanic rocks upper surface and the tertiary continental sediments, Hakrim, Heunghae, Idong, and Duho Formation upper surface and alluvium upper surface in study area.

Three-dimensional grid model composed of three-dimensional grid with total 2,046,000 deformable cells is constructed. The deformable cells are formed by hexahedron, which is fitted to the geologic formation boundary surfaces of three-dimensional structural model. These modeling result will can be used in various filed such as a geologic formation modeling, lithofacies or rock mass property modeling and flow simulation and others.

Three-dimensional geologic formation modeling is performed by integrating three-dimensional structural model and three-dimensional grid model in order to establish three-dimensional geologic formation model representing geologic formation and geologic features in study area. As a results of this modeling, It is confirmed that geologic formations of study area include the cretaceous plutonic rocks and volcanic rocks, and tertiary continental sediments that covered by these base rocks, Hakrim, Heunghae, Idong, and Duho Formation corresponding to marine sediments, and quaternary alluvium. Moreover, According to the result of the statistics

analysis, among eight geologic formations, volume of the cretaceous plutonic rocks is the most distributed one. Especially, among the tertiary formations corresponding to the Pohang Basin, the volume of Idong Formation is the most distributed.

Three-dimensional lithofacies modeling is performed in order to estimates and analyzes the distribution of lithofacies in uninvestigated area. As a result of this modeling, it is confirmed that variogram analysis result shows raw data have a good spatial correlation at azimuth 180° and dip 0° in study area. In addition, the result of SIS and TGS shows that the distribution of mudstone is dominating over the distribution of sandstone. The ratios of mudstone from TGS shows relatively small ratio compared with SIS result and the ratios of mudstone and sandstone from SIS are similar to raw data than the ratios of mudstone and sandstone from TGS.

Cross-validation is performed in order to assess the quality of the results of three-dimensional lithofacies modeling. As a result of cross-validation, it is confirmed that The borehole PY-2 excluded from Case S-4 and Case T-4 indicate the highest level of dependence among the six boreholes data for three-dimensional lithofacies modeling.

Through this study, three-dimensional geologic model shows that can be utilized for more realistic visualization and quantitative characterization of sedimentary basin in Pohang Basin. In addition, if there is more deep borehole data, it is expected that geologic structure or formation and lithofacies distribution can be predicted more realistically. Besides, it is expected that this study can be utilized effectively in various fields such as

groundwater flow, contaminant transport, resources exploration, carbon dioxide storage, radioactive waste disposal, and geothermal energy development.

References

Almeida, J.A. (2010), Stochastic simulation methods for characterization of lithoclasses in carbonate reservoirs, *Earth-Science Reviews*, 101, 250-270.

Christakos, G. (1984), On the problem of permeissible covariance and variogram models, *Water Resources Research*, 20, 251-265.

Deutsch, C.V. and A.G.Journel (1992), *GSLIB:Geostatistical Software Library and User's Guide*, 340 pp., Oxford University Press, Oxford, New York.

Fetel, E. and G. Caumon (2008), Reservoir flow uncertainty assessment using response surface constrained by secondary information, *Journal of Petroleum Science and Engineering*, 60, 170–180.

Goovaerts, P. (1996), Stochastic simulation of categorical variables using a classification algorithm and simulated annealing, *Mathematical Geology*, 28, 909–921.

Guyonnet-Benaize, C., J. Lamarche, J.P. Masse, M. Villeneuve, andS. Viseur (2010), 3D structural modelling of small-deformations in poly-phase fault pattern. application to the mid-cretaceous Durance uplift, Provence (SE France), *Joural of Geodynamics*, 50, 81-93.

Gwak, S.H. and D.S. Lee (2001), 3-D Visualization of reservoir characteristics through GOCAD, *Journal of The Korean Society of Earth and Exploration Geophysicists*, 4, 80-83 (in Korean with English abstract).

Han, J.H., Y.H. Kwak, J.D. Son, and B.K. Son (1987), Tectonic evolution and depositional environments of the tertiary sedimentary basin, southeastern part of Korea, *Korea Institute of Energy Research(KIER) Report*, KR-86-2-(B)-4, 109 pp.

Hwang, I.G. (1993), Fan-delta systems in the Pohang Basin (Miocene), SE Korea.Ph.D. thesis, Seoul National University, Seoul.973 pp (in Korean with English abstract).

Jeong, j. and W.I. Jang (2011), Estimation of distribution of the weak soil layer for using geostatistics, *Journal of the Korean society of Marine Engineering*, 35, 1132-1140 (in Korean with English abstract).

Journel, A.(1974), Geostatistics for conditional simulation of ore bodies,*Economic Geology*, 69, 673-687.

Journel, A.G. and C.J.Huijbergts (1978), *Mining Geostatistics*, 600 pp, Academic Press, London.

Kaufmann, O. and T. Martin (2009), Reprint of "3D geological modeling from boreholes, cross-sections and geological maps, application over former natural gas storages in coal mines", *Computers & Geosciences*, 35, 70-82.

Kim, S.J. and H.D. Park (2009), Development of software for mineral resoureestimation and 3D modeling using variogram, *Journal of The Korean society for Geosystem Engineering*, 46, 151-159 (in Korean with English abstract).

Kim, D.H., D.W. Ryu, J.H. Lee, I.G. Choi, J.K. Kim, and W.J. Lee (2010), Comparative studies of kriging methods for estimation of geo-layer distribution of Song-Do international city in Incheon, *Journal of Korean Society for Rock Mechanics*, 26, 57-64 (in Korean with English abstract).

Koo, C.M. and S.W.Jeon (2005), Using conditional simulation to estimate rock mass properties and assess the uncertainty, *Journal of The Korean Society for Rock Mechanics*, 3, 81-95 (in Korean with English abstract).

Koo, C.M., C.W.Hong, and S.W.Jeon (2006), Estimation of rock mass rating(RMR) and assessment of its uncertainty using conditional simulations, *Journal of The Korean Society for Rock Mechanics*, 16, 135-145 (in Korean with English abstract).

KIER (Korea Institute of Energy Research) (1987), Tectonic evolution and depositional

environments of the tertiary sedimentary basin, southeastern part of Korea, *Report KR-86-2-(B)-4*, 109 pp.

KIGAM (Korea Institute of Geoscience and Mineral Resources) (2003), Development of deep, low-enthalpy geothermal energy, *Report 03-1*, 85 pp.

KIGAM (Korea Institute of Geoscience and Mineral Resources) (2004), Development of deep, low-enthalpy geothermal energy, *Report 04-1*, 226 pp.

KIGAM (Korea Institute of Geoscience and Mineral Resources) (2005), Development of deep, low-enthalpy geothermal energy, *Report QAA2003001-2005(3)*, 147 pp.

KIGAM (Korea Institute of Geoscience and Mineral Resources) (2006), Development of deep, low-enthalpy geothermal energy, *Report QAA2003001-2006(4)*, 190 pp.

KOGS (Korea Office of Geological Survey) (1967), Geological and geophysical exploration for sign area of natural gas at Pohang, 44 pp.

Lee, S., Y.S.Kim, N.J. Kim, and K.H.Ahn (2008), Analysis of relationships between topography/geology and groundwater yield properties at Pohang using GIS, *Journal of The Korean Society of Economic and Environmental Geology*, 41, 115-131 (in Korean with English abstract).

Lee, C.B., T.K.Kim, and D.W.Park (2009), Geology and geochemistry of volcanic and sedimentary rock from deep borehole in the Heunghae area, North Kyungsang Province, *The journal of Engineering Geology*, 19, 459-474.

Louis, J.D.(2005), Upscaling and Gridding of Fine Scale Geological Models for Flow Simulation. International Forum on Reservoir Simulation, *Iles Borromees*, June 20-24, 59 pp, Stresa, Italy.

Matheron, G. (1963), Principles of geostatistics,*Economic Geology*, 58, 1246-1266.

Matheron, G., H.Beucher, C. Fouquet, A.Galli, E.M. Paris, D. Guerillot, C. Ravenne, and

F. Petrole (1987), Conditional simulation of the geometry of fluvio-deltaic reservoirs. *Society of Petroleum Engineers(SPE) Annual Technical Conference and Exhibition*, September 27-30, 591 pp, Dallas, Texas.

Mallet, J.L. (1989), Discretesmooth interpolation, *ACM transactions on Graphics*, 8, 212-144.

Shepard, D. (1968), A two-dimensional interpolation function for irregularly-spaced data, *ACM National Conference*,August 27-29, 517–524, New York.

Sohn, Y.K., C.W.Rhee and H. Sohn (2001), Revised stratigraphy and reinterpretation of the Miocene Pohang basin fills, SE Korea: sequence development in response to tectonic and eustassy in a back-are basin margin, *Sedimentary Geology*, 143, 265-285.

Vilain, D. (2010), 3D modelling and restoration of the Vargfors Basin, CertralSkellefte District, Northern Sweden, using gOcad and Move software, M.S. thesis, Lulea University of Technology, Lulea, Sweden, 19 pp.

Wang, G. and L. Huang (2012), 3D geological modeling for mineral resource assessment of the Tongshan Cu deposit, Heilongjiang Province, China, *GEOSCIENCE FRONTIERS*, 1-9.

Zanchi, A., S. Francesca, Z. Stefano, S. Simone, and G. Graziano (2007), 3D reconstruction of complex geological bodies: Examples from the Alps, *Computers & Geosciences*, 35, 49-69.

국문 초록 (Abstract in Korean)

한국 포항분지에 대해서 정량적으로 특성화하고 사실적으로 가시화하기 위하여 GOCAD 소프트웨어를 사용하여 삼차원 지질 모델링을 수행하였다. 연구 지역은 포항시 남구 해도동 일대로서 동서 1,200 m, 남북 2,200 m 및 심도 2,176 m에 해당한다. 먼저, 연구 지역에 위치하는 지리정보시스템과 대심도 시추공(A, B, C, DS-1, DS-2, PY-2, 301, 302)을 일차적으로 수집하고 분석하였다. 분석 결과 연구 지역에서 백악기 화성암층은 하부로부터 심성암층과 화산암층으로 나누어지며, 제3기 연일층군은 하부로부터 육성퇴적층과 해성퇴적층으로 나누어짐을 확인하였다. 그리고 제3기 해성퇴적층은 하부로부터 학림층, 홍해층, 이동층 및 두호층으로 나누어진다. 한편 연구 지역에는 단층 구조가 존재하지 않는다. 이러한 일차 분석 결과를 토대로 각 지층 경계면에 대해서 불연속 평활 보간법을 이용한 삼차원 구조 모델링을 수행하였다. 그리고 총 2,046,000개의 셀로 구성된 삼차원 격자 모델이 생성되었고, 이 두 모델들을 중합하는 삼차원 지층 모델링을 수행하였다. 아울러 삼차원 지층 모델의 각 지층 내 암상의 공간적 분포를 정량적으로 예측하고 평가하기 위하여 순차 지시 시뮬레이션과 절단 가우시안 시뮬레이션을 이용하여 삼차원 암상 모델링을 100회 수행하였다. 이때에 제3기 육성퇴적층 및

백악기 화산암층과 심성암층은 각각 역암 및 응회암과 화강암의 단일 암상으로 구성되어 있기 때문에 사암과 이암으로 구성되어 있는 제3기 해성퇴적층에 대해서만 삼차원 암상 모델링을 수행하였다. 삼차원 암상 모델링 결과는 제3기 해성퇴적층 내에서 이암이 사암에 비해서 압도적으로 많이 분포함을 보여준다. 그리고 통계분석 결과에 따르면, 절단 가우시안 시뮬레이션 결과는 순차 지시 시뮬레이션 결과보다 사암의 분포가 적음을 보여준다. 또한 절단 가우시안 시뮬레이션을 사용했을 때보다 순차 지시 시뮬레이션을 사용했을 때 이암과 사암의 부피비가 원시 자료와 더 유사함을 보여준다. 그리고 예측된 삼차원 암상 모델에 대한 우수성을 평가하기 위하여 교차 검증을 수행하였다. 그 결과는 삼차원 암상 모델링에 사용된 6개의 시추공중에서 PY-2 시추공이 본 연구에 가장 높은 의존도를 보여주었다.

주요어 : 포항분지, 삼차원 지질 모델링, 지구통계학, 순차 지시 시뮬레이션, 절단 가우시안 시뮬레이션, 교차 검증

학 번 : 2011-20371

.